

SHEAR VISCOSITY OVER ENTROPY DENSITY CALCULATION IN HEAVY ION COLLISION

Bidisha Biswas
Roll No: MS16011

*A dissertation submitted for the partial fulfilment
of BS-MS dual degree in Science*

Under the guidance of
Dr. Satyajit Jena



May, 2021


Indian Institute of Science Education and Research Mohali
Sector - 81, SAS Nagar, Mohali 140306, Punjab, India

Certificate of Examination

This is to certify that the dissertation titled “**Shear viscosity over entropy density ratio calculation in heavy ion collision**” submitted by **Bidisha Biswas** (Reg. No. MS16011) for the partial fulfillment of BS-MS dual degree programme of the Institute, has been examined by the thesis committee duly appointed by the Institute. The committee finds the work done by the candidate satisfactory and recommends that the report be accepted.



Dr. Ambresh Shivaji



Dr. Vishal Bhardwaj



Dr. Satyajit Jena
(Supervisor)

Dated: 26.05.2021

Declaration

The work presented in this dissertation has been carried out by me under the guidance of Dr. Satyajit Jena at the Indian Institute of Science Education and Research Mohali.

This work has not been submitted in part or in full for a degree, a diploma, or a fellowship to any other university or institute. Whenever contributions of others are involved, every effort is made to indicate this clearly, with due acknowledgment of collaborative research and discussions. This thesis is a bonafide record of original work done by me and all sources listed within have been detailed in the bibliography.



Bidisha Biswas

(Candidate)

Dated: May 26, 2021

In my capacity as the supervisor of the candidate's project work, I certify that the above statements by the candidate are true to the best of my knowledge.



Dr. Satyajit Jena

(Supervisor)

Acknowledgement

First and foremost, I would like to thank my thesis supervisor Dr. Satyajit Jena, without whose help and supervision, this thesis would have never been possible. The discussions that I had with him has enhanced my capabilities as a researcher.

I would also like to thank my thesis committee members Dr.Ambresh Shivaji and Dr. Vishal Bhardwaj for their valuable suggestions and criticism of my work.

I owe my deepest gratitude to Rohit Gupta for helping me with the discussions and data collection. My labmates owe special thanks for always encouraging me and providing a homely environment in the lab. I want to acknowledge the moral support and encouragement that I have continuously received from my parents.

Finally, I am thankful to IISER Mohali for providing me with a wonderful infrastructure, Library and Computer Centre for all the technical support. I would also like to acknowledge DST-INSPIRE, the Government of India, for the financial support.

Bidisha Biswas

MS16011

IISER Mohali.

List of Figures

| | | |
|------|--|----|
| 1.1 | Strong coupling constant as a function of the energy scale [34] | 3 |
| 1.2 | Formation of QGP [20] | 4 |
| 1.3 | An almond shape formation in Pb-Pb non-central collision. Spatial anisotropy with respect to reaction (x-z) plane leads to momentum anisotropy of the scattered produced particles [19] | 5 |
| 1.4 | A schematic of evolution stages of RHIC [1] | 8 |
| 1.5 | Left side plot shows $\pi^+ + \pi^-$ (total) p_T distribution and right side plot denotes p_T distribution for π^+ and π^- separately at $\sqrt{s_{NN}} = 2.76$ TeV for all centralities in Pb-Pb collisions | 10 |
| 1.6 | Left side plot shows $\pi^+ + \pi^-$ (total) p_T distribution and right side plot denotes p_T distribution for π^+ and π^- separately within $ \eta < 0.8$ range at $\sqrt{s_{NN}} = 2.76$ TeV for all centralities in Pb-Pb collisions | 11 |
| 1.7 | Left side plot shows $\pi^+ + \pi^-$ (total) y distribution and right side plot denotes y distribution for π^+ and π^- separately at $\sqrt{s_{NN}} = 200$ TeV for all centralities in Pb-Pb collisions | 11 |
| 1.8 | Left side plot shows all charged particles η distribution and right side plot denotes η distribution for positive and negative charged particles separately at $\sqrt{s_{NN}} = 2.76$ TeV for all centralities in Pb-Pb collisions | 12 |
| 1.9 | A schematic decomposition of particle momentum \vec{p} into parallel and longitudinal components and angle of emitted particle: i.e polar angle (θ) and azimuthal angle (ϕ) [29] | 12 |
| 1.10 | Left side plot shows $\pi^+ + \pi^-$ (total) ϕ distribution and right side plot denotes for π^+ and π^- separately at $\sqrt{s_{NN}}=2.76$ TeV in Pb-Pb collisions for 0-5 % centrality | 13 |

| | | |
|------|---|----|
| 1.11 | Left side plot shows $\pi^+ + \pi^-$ (total) ϕ distribution and right side plot denotes ϕ distribution for π^+ and π^- separately within $ \eta < 0.8$ range at $\sqrt{s_{NN}} = 2.76$ TeV in Pb-Pb collisions for 0-5 % centrality | 13 |
| 1.12 | Left side plot shows $\pi^+ + \pi^-$ (total) ϕ distribution and right side plot denotes ϕ distribution for π^+ and π^- separately at $\sqrt{s_{NN}} = 2.76$ TeV in Pb-Pb collisions for 95-100 % centrality | 14 |
| 1.13 | Left side plot shows $\pi^+ + \pi^-$ (total) ϕ distribution and right side plot denotes ϕ distribution for π^+ and π^- separately within $ \eta < 0.8$ range at $\sqrt{s_{NN}} = 2.76$ TeV in Pb-Pb collisions for 95-100 % centrality | 14 |
| 4.1 | $\pi^+ + \pi^-$ (total) p_T distribution fitted with Tsallis for Pb-Pb collision energy at $\sqrt{s_{NN}} = 2.76$ TeV with $ \eta \leq 0.5$ for different centrality (for UrQMD data) | 34 |
| 4.2 | $K^+ + K^-$ (total) p_T distribution fitted with Tsallis for Pb-Pb collision energy at $\sqrt{s_{NN}} = 2.76$ TeV with $ \eta \leq 0.5$ for different centrality (for UrQMD data) | 36 |
| 4.3 | shear viscosity as varying $\langle N_{part} \rangle$ for $\pi^+ + \pi^-$ (total) p_T produced in Pb-Pb collision at $\sqrt{s_{NN}} = 2.76$ TeV with $ \eta \leq 0.5$ for UrQMD data | 37 |
| 4.4 | shear viscosity as varying $\langle N_{part} \rangle$ for $K^+ + K^-$ (total) p_T produced in Pb-Pb collision at $\sqrt{s_{NN}} = 2.76$ TeV with $ \eta \leq 0.5$ for UrQMD data | 37 |
| 4.5 | entropy density as varying $\langle N_{part} \rangle$ for $\pi^+ + \pi^-$ (total) p_T produced in Pb-Pb collision at $\sqrt{s_{NN}} = 2.76$ TeV with $ \eta \leq 0.5$ | 38 |
| 4.6 | entropy density as varying $\langle N_{part} \rangle$ for $K^+ + K^-$ (total) p_T produced in Pb-Pb collision at $\sqrt{s_{NN}} = 2.76$ TeV with $ \eta \leq 0.5$ for UrQMD data | 38 |
| 4.7 | shear viscosity over entropy density ratio as varying $\langle N_{part} \rangle$ for $\pi^+ + \pi^-$ (total) p_T produced in Pb-Pb collision at $\sqrt{s_{NN}} = 2.76$ TeV with $ \eta \leq 0.5$ for UrQMD data | 39 |
| 4.8 | shear viscosity over entropy density ratio as varying $\langle N_{part} \rangle$ for $K^+ + K^-$ (total) p_T produced in Pb-Pb collision at $\sqrt{s_{NN}} = 2.76$ TeV with $ \eta \leq 0.5$ for UrQMD data | 39 |

List of Tables

| | | |
|-----|--|----|
| 4.1 | $\langle N_{part} \rangle$ for each centrality class | 30 |
| 4.2 | Centrality wise Freeze-out parameters after fitting p_T spectra with Tsallis distribution for π^\pm for UrQMD data of Pb-Pb collision at $\sqrt{s_{NN}} = 2.76$ TeV | 31 |
| 4.3 | Centrality wise Freeze-out parameters after fitting p_T spectra with Tsallis distribution for K^\pm for UrQMD data of Pb-Pb collision at $\sqrt{s_{NN}} = 2.76$ TeV | 32 |

Contents

| | |
|--|-----------|
| Acknowledgement | i |
| List of Figures | iv |
| List of Tables | v |
| Abstract | ix |
| 1 Introduction | 1 |
| 1.1 Quantum Chromo Dynamics | 2 |
| 1.1.1 Properties of QCD | 2 |
| 1.2 Conceptual basis for QGP formation | 4 |
| 1.3 Probing QGP | 4 |
| 1.4 High Energy Heavy-Ion Collision in QGP | 7 |
| 1.4.1 Evolution of Collision | 7 |
| 1.5 Kinematics | 8 |
| 1.5.1 Transverse Momentum Distribution | 9 |
| 1.5.2 Rapidity Distribution | 9 |
| 1.5.3 Azimuthal Angle Distribution | 12 |
| 1.5.4 Collision Centrality | 14 |
| 2 Hydrodynamics | 17 |
| 2.1 Formulation of Relativistic Hydrodynamics | 17 |
| 2.1.1 Prequistics | 17 |
| 2.1.2 Relativistic Hydrodynamics from kinetic theory | 18 |
| 2.2 Relativistic Hydrodynamics Equation of Motion | 19 |
| 2.3 Applicability and length scale of Hydrodynamics | 20 |

| | | |
|----------|---|-----------|
| 3 | Various modes for calculating shear viscosity over entropy density ratio | 21 |
| 3.1 | UrQMD Box Calculation | 22 |
| 3.2 | Viscosity of Gas in Classical Approach | 22 |
| 3.3 | Formulation of Viscosity of Hadron Gas | 23 |
| 3.4 | Formulation of Viscosity from Hydrodynamical Approach | 24 |
| 3.5 | Entropy Density | 26 |
| 4 | Result and Conclusion | 29 |
| 4.1 | Charged Pion Characteristics | 29 |
| 4.2 | Charged Kaon Characteristics | 29 |
| 4.3 | Computation | 30 |
| 5 | Summary and Conclusion | 41 |
| A | Simulating the Events: Technical Part | 43 |
| | Bibliography | 44 |

Abstract

In Heavy Ion Collision Quark-Gluon Plasma(QGP) are formed, and at extremely dense conditions, it behaves like a superfluid, but unfortunately, we do not have complete access to its properties like temperature, equation of state, transport co-efficient etc., we are only able to get the information about the spectra of final state particles. QGP is also characterized by a very small shear viscosity to entropy density ratio (η/s), which is predicted as a lower bound with the help of Anti-deSitter space/Conformal Field (Ads/CFT) theory and it is expected to be within 0.08-0.24 range with different initial conditions. While trying to reconstruct QGP like phenomena in a lab environment, we will work with relativistic heavy-ion collision (RHIC) particularly, Pb-Pb collisions in $\sqrt{s_{NN}} = 2.76$ TeV. In the context of RHIC, the study of shear viscosity is significant as it drives a non-equilibrium system towards its equilibrium. The equilibration of momentum anisotropy, converted from spatial anisotropy in the nuclear collision, is one of the crucial aspects that govern by shear viscosity co-efficient. In the evolution of RHIC, as the system in QGP state expands and cools off, it tries to get through a phase transition from quark-gluon to hadronic gas phase with a rapid increase in η/s . We calculate the quantity - η/s as a function of varying centrality to verify the lower value predicted for QGP also holds for hadron gas. We also try to observe if centrality (or impact parameter) for a particular type of collision does have any effect on η/s value for hadron gas.

Chapter 1

Introduction

What is Quark-Gluon Plasma (QGP)? Before searching for an answer to the above question, we would like to know what quarks and gluons are. For many decades, right after discovering neutrons in 1932 by James Chadwick, it was assumed that protons, neutrons and electrons are the fundamental blocks of elementary particles. But in 1964, two physicists, Murray Gell-Mann and George Zweig independently proposed the quark model where the protons and neutrons can be further divided into the substructure called quarks. The quark model was later well established after finding out their physical existence in deep inelastic electron-proton scattering experiments at the Stanford Linear Accelerator Center in 1968. So, now quarks are believed to be one of the primary constituents of matter. Quarks have some intrinsic properties like mass, electric charge, color charge, and spin. They are of six types, known as flavours - up (u), charm (c), bottom (b), down (d), strange (s), and top (t). Up and down quarks have lower masses and are generally stable, so they are more common in nature, whereas strange, charm, bottom, and top quarks are heavier and can only be produced in very high energy collisions. For every quark flavor, there is an antiparticle of their corresponding type, known as an antiquark. Protons are made up of two up-quarks and one down-quark, whereas neutrons are made up of two down-quarks and one up-quark. If these hadrons are formed by accumulating quarks, then our next question should be how these hadrons are formed? What forces are involved there? Basically, there are four fundamental forces - the strong force, the weak force, the electromagnetic force and the gravitational force. Among all of them in nuclear region, strong force is much more dominant and in the strong force as force carrier, gluons are introduced. Gluons are another sets of elementary particles that act as the exchange particle for the strong force between quarks and glue the

quarks together into hadrons. The experiments find the first direct proof of the existence of gluons at the DESY laboratory in Germany in 1979. This legendary discovery created a milestone in the history of particle physics, as it helped to establish the theory of the strong force, called quantum chromodynamics, very firmly. Quarks and gluons are collectively called ‘partons’. Because the strong force in the nuclear regime is compelling, it is practically impossible to separate two quarks. Then does it mean that we can not achieve free quark? Here comes the importance of QGP. To separate two quarks, we need to create a state of matter which is called QGP. It has formed in the early universe for few fractions of a second.

Collins and Perry already discussed the physics of Quark gluon plasma (QGP) at extreme conditions of temperature and very high density before 1975. But the term ‘QGP’ is coined by Russian-American physicist E. V. Shuryak in 1980. Quark gluon plasma is a state of matter which exist at extremely high temperature and density and consists of an extremely hot and dense soup of quarks (fermions) and gluons (bosons). But before going to QGP in detail, we need to briefly go through the theory that explains the dynamics of QGP, i.e; QCD (Quantum Chromo Dynamics).

1.1 Quantum Chromo Dynamics

In QCD, color charge comes into the picture. QCD is the theory that includes the strong interaction between quarks. As leptons do not have color charge, they do not interact through strong interaction. Quarks can have three type of colors-‘red’, ‘blue’, ‘green’, and their antiparticles likewise carry anticolors. Gluons are bicolored and carry both positive and negative color in a set - so there are eight possible combinations of gluons that have been found. While drawing the Feynman diagram, unlike QED here in each vertex, due to the change in separation between interacting particles, coupling constant varies and it becomes an important property of QCD.

1.1.1 Properties of QCD

- **Quark Confinement:** After being hit by some energetic particles, if a quark starts to move away from another neighbour quark, the mediating gluons will use the energy to produce more gluons. The momentum transfer between those quarks by exchange-

ing more gluons will become high. Thus the strength of the strong force will be enhanced so that at some time, the energy to produce additional quark-antiquark pair as a meson or baryon will be achieved before those quarks get separated from their constituent. Hence we can never get an isolated quark in a normal scenario. This is ‘Quark Confinement’.

- **Asymptotic freedom:** At very high density or high temperature, when two quarks are brought so close that they lose their individuality and interact with each other very weakly, they are treated as quasi-free particles. This property of QCD is ‘Asymptotic Freedom’. This phenomena is seen in high energy heavy ion collisions.
- **Running coupling constant:** Above two properties can be well explained by using another property of QCD - ‘Running coupling constant’.

$$\alpha_s(Q^2) = \frac{1}{\beta_0 \ln \left(\frac{Q^2}{\Lambda^2} \right)} \quad (1.1)$$

where Q^2 = available energy, Q = momentum carried by the gluons, Λ = QCD scale or compared value between QCD predictions and experimental results, β_0 = beta function in QCD.

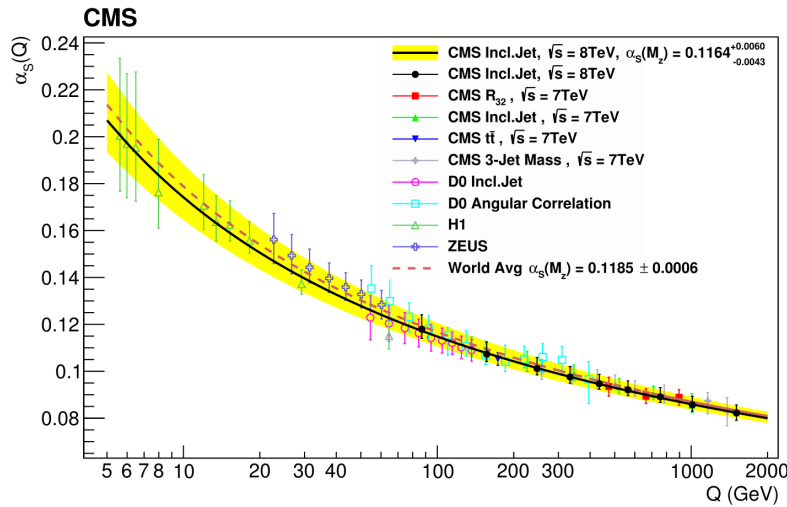


Figure 1.1: Strong coupling constant as a function of the energy scale [34]

From fig 1.1 as well as equation 1.1 we can see for low Q , as the momentum transfer between two quarks become low, the coupling constant becomes higher, strength of strong force becomes high and results in ‘quark-confinement’.

In high energy for high Q , as the momentum transfer between two quarks become high, the coupling constant becomes lower, strength of strong force become low and results in ‘quark-deconfinement’ and thus ‘asymptotic freedom’ is observed. We can also explain confinement-deconfinement phase transition or vice-versa through ‘Running Coupling Constant’.

1.2 Conceptual basis for QGP formation

Quark gluon plasma is a state of matter in QCD that exist at extremely high temperature and density. At high density, the concept of hadronic matter loses its identity, i.e., the quarks inside a hadron fail to recognize their partner quarks, as, at high density, the distance between two foreign quarks becomes smaller than the hadronic radius. However, similar phenomena can happen at high temperature. In this case, as the temperature of the system increases, more low mass hadrons (primarily pions) are produced so again, the density goes higher, and confinement to deconfinement phase transition happens- QGP forms. It is calculated that beyond a definite critical energy density, i.e., $\sim 1 \text{ GeV}/fm^3$ or temperature $\sim 200 \text{ MeV}$, matter can exist only as QGP [10].

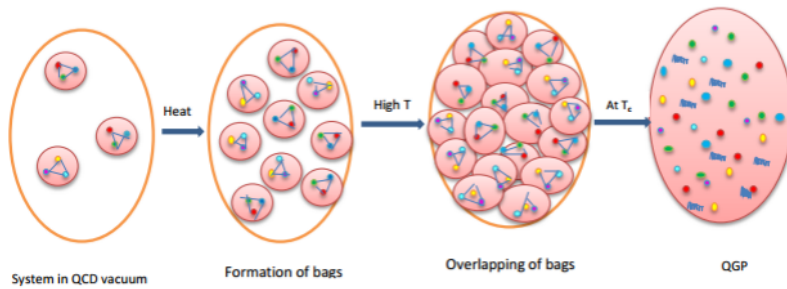


Figure 1.2: Formation of QGP [20]

1.3 Probing QGP

In the heavy-ion collisions, the final state particles can only be detected then, how can we certain about whether QGP is formed in the medium or not. At high temperature or density,

strongly interacting matter will be in a new state (namely QGP) and to study the properties of this state we can rely on a certain number of indirect signals [13]:

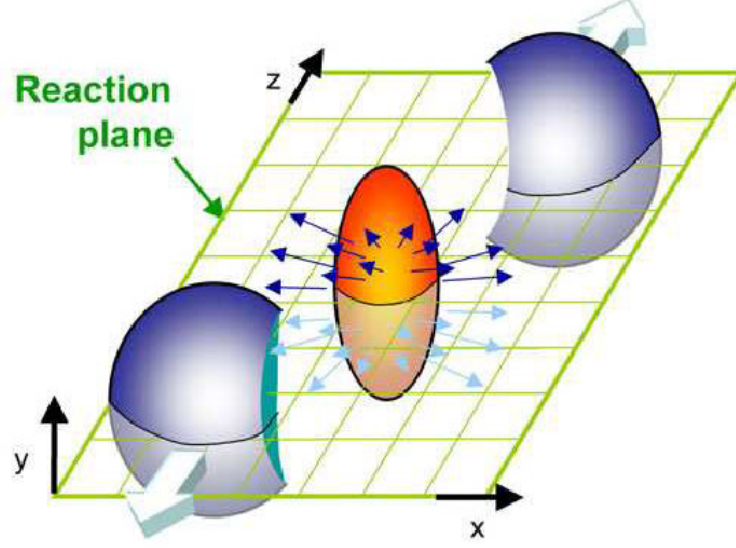


Figure 1.3: An almond shape formation in Pb-Pb non-central collision. Spatial anisotropy with respect to reaction (x-z) plane leads to momentum anisotropy of the scattered produced particles [19]

1. **Elliptic Flow:** Elliptic flow captures the momentum anisotropy in sub-atomic particles. In non-central collision (where the impact parameter is non-zero), the initial reaction zone already possesses a spatial anisotropy due to azimuthal anisotropy. In this situation, when a thermalized system begins to evolve due to the pressure gradient, the expansion will not be uniform as we can observe in fig 1.3 that particle flow will be greater along minor axis than major axis, resulting in an unequal distribution of unequal momentum distribution of the produced particles. The types of anisotropic flow can be shown by the Fourier expansion of the Lorentz invariant differential yield distribution [35]:

$$E \frac{d^3N}{d^3p} = \frac{1}{2\pi} \frac{d^2N}{p_T dp_T dy} \left(1 + 2 \sum_{n=1}^{\infty} v_n \cos(n(\phi - \psi_{RPA})) \right) \quad (1.2)$$

where E = energy of the particle, p = momentum of partons, p_T = transverse momentum, ϕ = azimuthal angle, y = rapidity, and ψ_{RPA} = reaction plane angle, v_n = flow coefficients. Here v_1 = directed flow, v_2 = elliptic flow, v_3 = triangular flow. Among all flows, elliptic flow is the strong proof of QGP's existence.

2. **Jet Quenching:** In the heavy-ion collision, the participating partons get highly accelerated. When such accelerated parton from a nucleon scatters off parton from another nucleon, it forms a parton shower which hadronizes and leads to a collimated ray of hadrons [23]. These collimated beams are jets. Now, when a jet travels through a QGP medium, it loses its energy - that is called Jet Quenching. Usually, Nuclear Modification Factor (R_{AA}) measures jet quenching. If $R_{AA} = 1$ then no quenching happens; if $R_{AA} < 1$ then quenching occurs and QGP has formed.
3. **Net Charge Fluctuation:** It is anticipated that the net charge fluctuation is proportional to the squared value of electric charge that is significantly different for the QGP phase and hadronic phase [6]. If the unit of charge (Q) is 1, then it is in the hadronic phase, and if it is $1/3$, then it is in the QGP phase. So, while going through a phase transition, it is expected to see different fluctuations in net charge depending on the phase.
4. **Hadron radiation:** As an unknown hot and dense medium radiates, we can study the emission of hadrons consisting of light (u, d, s) quarks, but as they produced from transition surface between QGP and physical vacuum, they lost the information of unknown medium; thus if we want to know we have to allow the medium to expand freely without any constraints and as it expands and cools down this leads to hydrodynamic flow that gives an added boost to radiated hadrons and this radial flow (elliptic flow) will incorporate the initial energy density. In this way, we can get the information about pre-hadronic phase.
5. **Electromagnetic radiation:** The unknown hot medium also radiates photons and dileptons (e^+e^- , $\mu^+\mu^-$) and as they are produced electromagnetically, they emit immediately after production so, the inspection of their spectra can tell the state of the unknown medium at the place or the time they were formed. But they also can be formed anywhere, like cool surface or by the emitted hadrons. So, there is some uncertainty in this process.
6. **Dissociation of a passing quarkonium beam:** We expect that the different charmonium states have different “melting temperatures” in a QGP; therefore, shooting the known charmonium beams inside the medium and collecting the spectra can roughly estimate its temperature.

1.4 High Energy Heavy-Ion Collision in QGP

In the early universe, after few microseconds of the Big Bang, it is believed that QGP has been formed for a few millionths (≈ 10 ps) of a second and froze out into final state particles after about $10 \mu s$, which are the hadrons that we see now. We can recreate similar phenomena in the lab with the help of powerful accelerators. Suppose beams of two ultrarelativistic heavy ions, such as gold (Au) or lead (Pb) nuclei, collide with each other at higher relative velocities and achieve high energy density or high temperature (10^{12} K). In that case, QGP-like phenomena (named as little bang) is seen to be formed. The first evidence for jets was seen in 2003 in the STAR and PHENIX experiments at Brookhaven National Laboratory's (BNL) Relativistic Heavy Ion Collider (RHIC) in the US in heavy-ion collisions.

1.4.1 Evolution of Collision

Each incident nucleus is seen as a Lorentz-contracted disc and they collide into each other - collision can be two type, central (impact parameter, $b \sim 0$; here all are participants) and non-central or peripheral (impact parameter, $0 < b < 0$ diameter of nucleus, if two colliding nuclei are of same radius; here some are participants).

- **Pre-equilibrium:** After beams of two heavy-ions collide with each other, the partons are produced and scattered among each other. In this stage, the higher transverse momentum (p_T) particles and a large amount of real or virtual photons are produced.
- **Thermalization:** The partons come to a local thermal equilibrium (thermalized state) through elastic as well as inelastic collision among each other. New flavour compositions are formed by inelastic collision. In this state, the system has an internal thermal pressure and outside is the vacuum. Due to the pressure difference between the system and outside, the system initially begins to expand. Here some of the partons convert into hadrons-this is called the 'mixed phase'.
- **Hadronization and Chemical freeze out:** As the system evolves, the temperature as well as the energy density decreases and at a critical temperature ($T_{cr} \approx 170$ MeV) or critical energy density ($\epsilon_{cr} \approx 1 \text{ GeV} \cdot \text{fm}^{-3}$), deconfinement-confinement QCD phase transition [14], [38], [32] happens and new hadrons are formed from partons. When

all the partons are converted into hadrons or hadronization has been completed - this is called ‘Chemical Freeze-out’. Here the flavour composition of QGP remains fixed.

- **Kinetic Freeze out:** The hadrons still interact with each other through elastic collision and try to achieve local equilibrium. In this stage, the system further expands and cools down until the mean free path between two hadronic collisions are greater than the radius of strong interaction. At this moment, elastic collision also cease to exist, and the hadrons decouple or freeze-out - widely known as ‘Kinetic Freeze-out’. After that, particles are detected through the detectors.

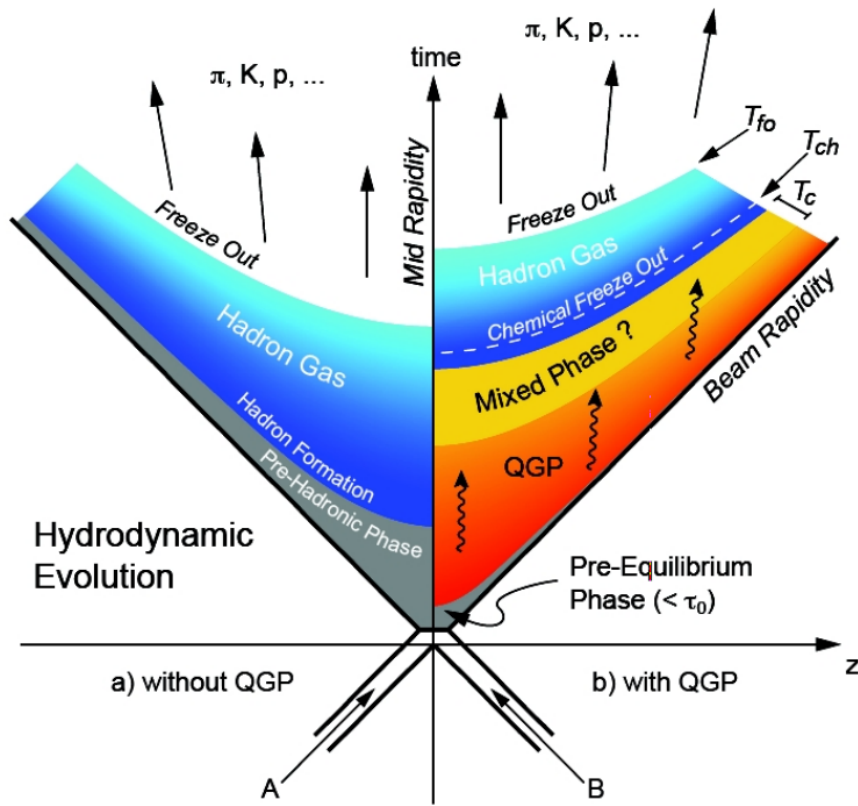


Figure 1.4: A schematic of evolution stages of RHIC [1]

1.5 Kinematics

We can find the exact parametric solutions for ideal hydrodynamics to describe RHIC. The exact solution of hadronic observables does not depend on the initial state, rather depends

on the final state. From the equation, we can extract momentum distribution, elliptic flow and Bose-Einstein correlation radii and fit it to actual observation; the fitted parameters of the solution describe the hadronic freeze-out.

1.5.1 Transverse Momentum Distribution

The transverse momentum (p_T) of a particle is defined by:

$$p_T = \sqrt{p_x^2 + p_y^2} \quad (1.3)$$

where p_x and p_y are the momentum components in the transverse momentum plane. Transverse momentum spectra of final state particles are the first observation in high energy experiments. If we fit the observed data to the Tsallis distribution, we can able to find the freeze-out temperature (T). Other than the freeze-out temperature, we could extract information about radial flow from transverse momentum distribution as in a heavy-ion collision, radial flow plays an important role in getting to know about the expansion of fireball and the initial pressure produced just after the collision. Graphically for p_T distribution in x-axis we put p_T and in y-axis the Lorentz invariant yield ($\frac{E d^3 N}{d^3 p}$) and it can be expressed as:

$$E \frac{d^3 N}{d p^3} = \frac{d^2 N}{2\pi |\vec{p}_T| d p_T d y} \quad (1.4)$$

where $d^2 N$ is the number of particles in a particular p_T bin in particular rapidity range. Now p_T distribution graphs for charged pion particles are below :

1.5.2 Rapidity Distribution

In relativistic energy rapidity variable is defined by [10]:

$$\begin{aligned} y &= \frac{1}{2} \ln \left(\frac{E + p_z}{E - p_z} \right) \\ &= \tanh^{-1} \left(\frac{p_z}{E} \right) \\ &= \frac{1}{2} \ln \left(\frac{\sqrt{\vec{p}^2 + m^2} + p \cos \theta}{\sqrt{\vec{p}^2 + m^2} - p \cos \theta} \right) \end{aligned} \quad (1.5)$$

If the particles are boosted along longitudinal direction (z axis or beam axis) and they are emitted at an angle θ with respect to the beam axis, $p_z = p \cos \theta$, m , E are respectively mass and energy of the particle.

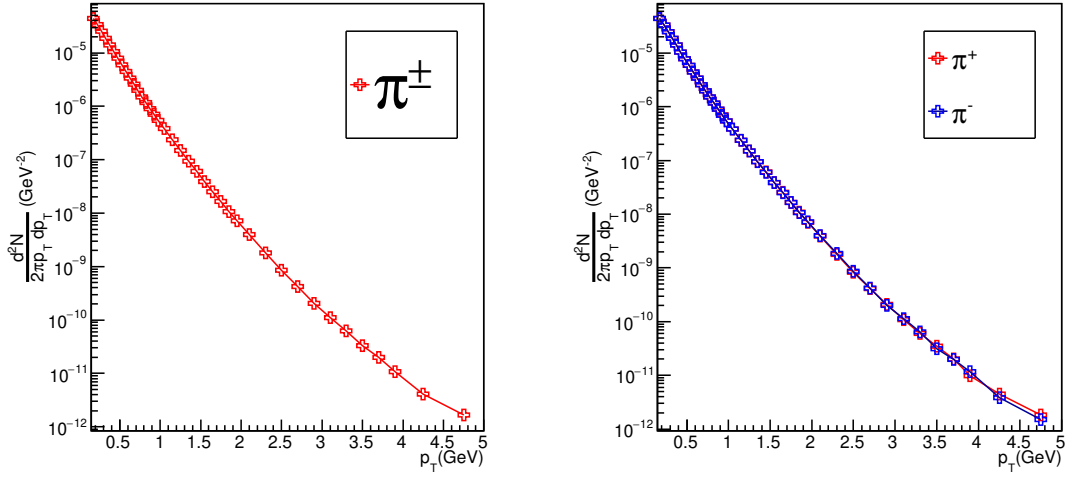


Figure 1.5: Left side plot shows $\pi^+ + \pi^-$ (total) p_T distribution and right side plot denotes p_T distribution for π^+ and π^- separately at $\sqrt{s_{NN}} = 2.76$ TeV for all centralities in Pb-Pb collisions

At very high energy limit i.e; $p \gg m$, the mass can be neglected:

$$\begin{aligned}
 y &= \frac{1}{2} \ln \left(\frac{p + p \cos \theta}{p - p \cos \theta} \right) \\
 &= -\ln(\tan \theta / 2) \\
 &= \eta
 \end{aligned} \tag{1.6}$$

here η is called pseudorapidity and it is only dependent on angle θ . For unidentified particle we take η as we do not know its rest-mass, while for identified particles, we always take y distribution into account. But for both distributions the shape is independent of the frame of reference.

The distribution of particles as a function of rapidity is related to that of pseudorapidity by the formula:

$$\frac{dN}{d\eta dp_T} = \sqrt{1 - \frac{m^2}{m_T^2} \cosh^2 y} \frac{dN}{dy dp_T} \tag{1.7}$$

where transverse mass (m_T) of a particle is defined by:

$$m_T = \sqrt{m^2 + p_T^2} \tag{1.8}$$

For $y \gg 0$ region rapidity distribution ($\frac{dN}{dy}$, integration over all p_T) and pseudo-rapidity distribution ($\frac{dN}{d\eta}$, integration over all p_T) are almost same, but in the region $y \approx 0$; $\cosh y \rightarrow$

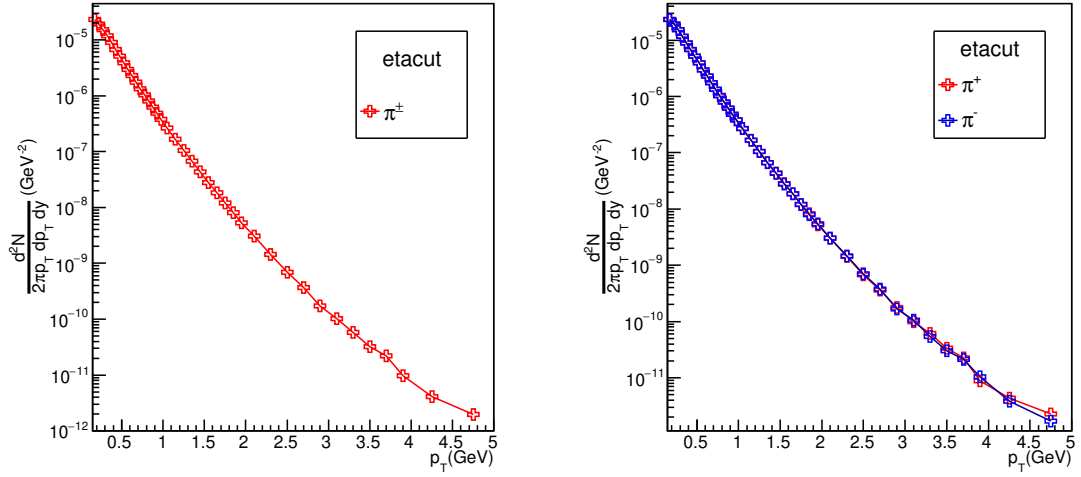


Figure 1.6: Left side plot shows $\pi^+ + \pi^-$ (total) p_T distribution and right side plot denotes p_T distribution for π^+ and π^- separately within $|\eta| < 0.8$ range at $\sqrt{s_{NN}} = 2.76$ TeV for all centralities in Pb-Pb collisions

0 the complexity arises. In that region there is a small depression in $\frac{dN}{d\eta}$ distribution compared to $\frac{dN}{dy}$ distribution due to the 1.7 transformation. But for massless particles like photons the shape of two distributions is expected to be same.

Now for y and η distribution for charged pions and all charged particles respectively are below:

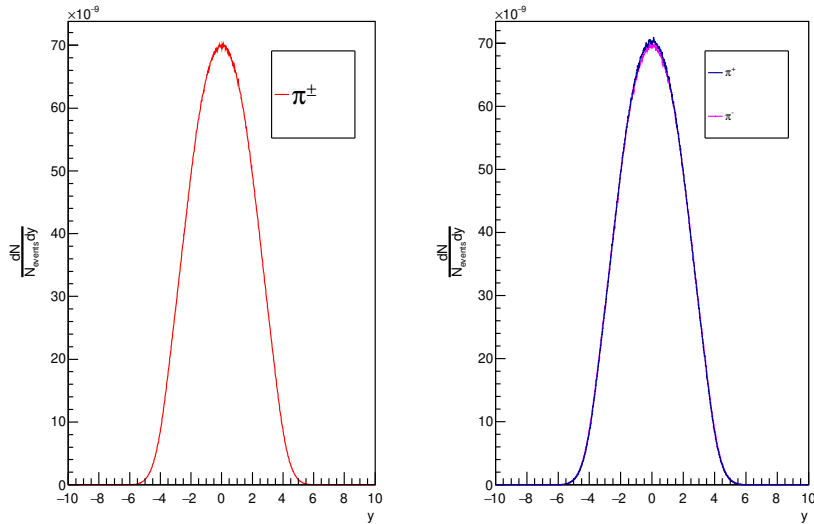


Figure 1.7: Left side plot shows $\pi^+ + \pi^-$ (total) y distribution and right side plot denotes y distribution for π^+ and π^- separately at $\sqrt{s_{NN}} = 200$ TeV for all centralities in Pb-Pb collisions

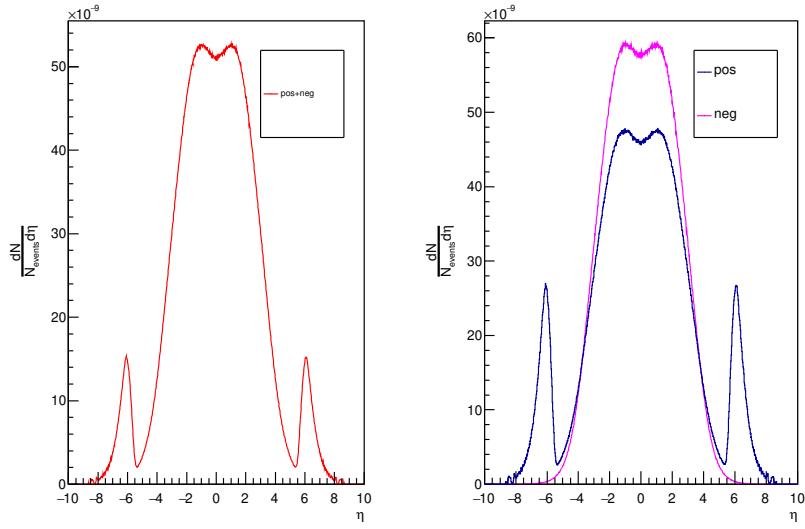


Figure 1.8: Left side plot shows all charged particles η distribution and right side plot denotes η distribution for positive and negative charged particles separately at $\sqrt{s_{NN}} = 2.76$ TeV for all centralities in Pb-Pb collisions

1.5.3 Azimuthal Angle Distribution

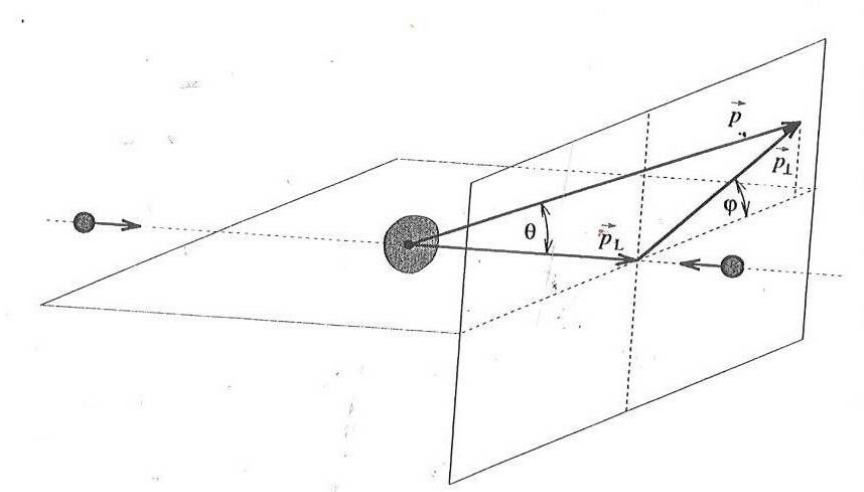


Figure 1.9: A schematic decomposition of particle momentum \vec{p} into parallel and longitudinal components and angle of emitted particle: i.e polar angle (θ) and azimuthal angle (ϕ) [29]

In a collider two particles or beam collides in the beam axis (mostly z axis) and particles are emitted from the collision point making a polar angle θ with the beam axis and azimuthal angle ϕ in the transverse plane (x-y plane). After getting the information of each momentum component of produced particle we can write azimuthal angle for each particle as:

$$\phi = \tan^{-1}\left(\frac{p_x}{p_y}\right) \quad (1.9)$$

The azimuthal distribution should be uniform from 0 to 2π range. Now for ϕ distribution for charged pions are below:

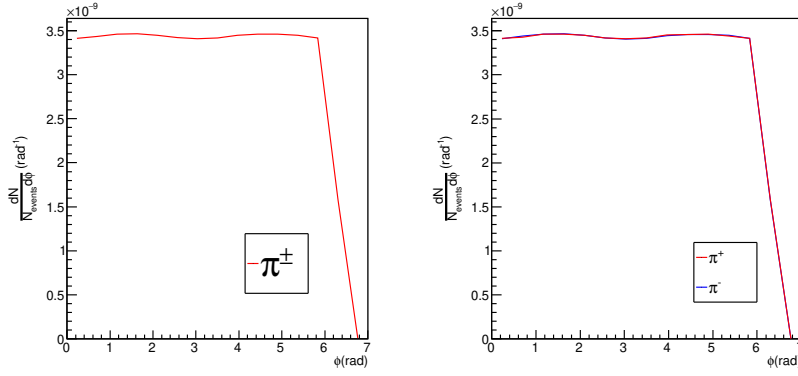


Figure 1.10: Left side plot shows $\pi^+ + \pi^-$ (total) ϕ distribution and right side plot denotes for π^+ and π^- separately at $\sqrt{s_{NN}}=2.76$ TeV in Pb-Pb collisions for 0-5 % centrality

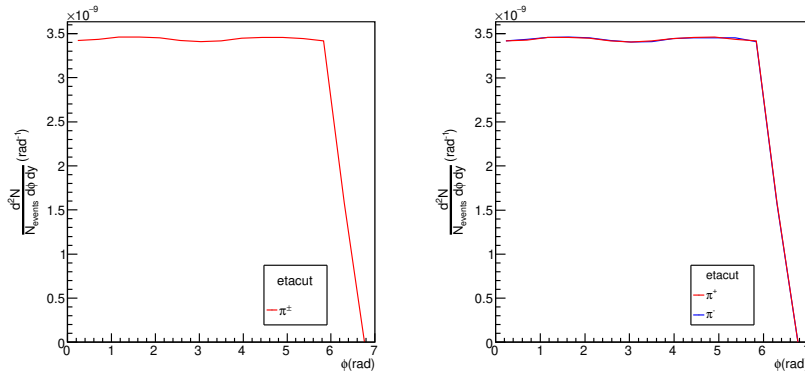


Figure 1.11: Left side plot shows $\pi^+ + \pi^-$ (total) ϕ distribution and right side plot denotes ϕ distribution for π^+ and π^- separately within $|\eta| < 0.8$ range at $\sqrt{s_{NN}} = 2.76$ TeV in Pb-Pb collisions for 0-5 % centrality

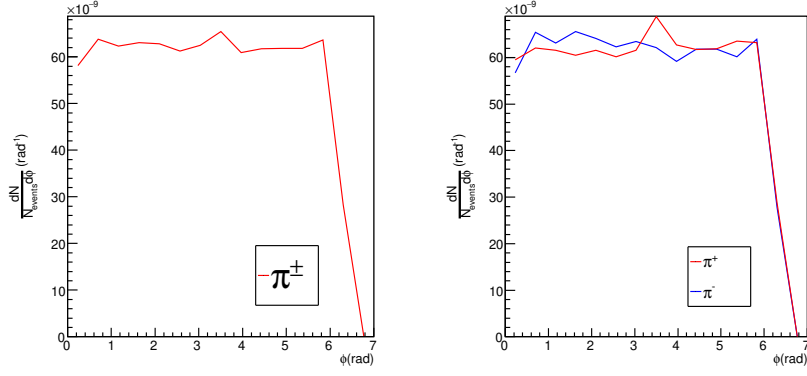


Figure 1.12: Left side plot shows $\pi^+ + \pi^-$ (total) ϕ distribution and right side plot denotes ϕ distribution for π^+ and π^- separately at $\sqrt{s_{NN}} = 2.76$ TeV in Pb-Pb collisions for 95-100 % centrality

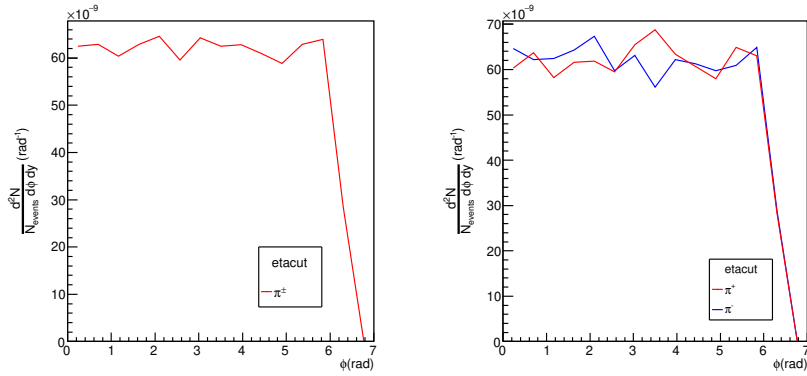


Figure 1.13: Left side plot shows $\pi^+ + \pi^-$ (total) ϕ distribution and right side plot denotes ϕ distribution for π^+ and π^- separately within $|\eta| < 0.8$ range at $\sqrt{s_{NN}} = 2.76$ TeV in Pb-Pb collisions for 95-100 % centrality

1.5.4 Collision Centrality

The nucleus is not a point object, so depending on the impact parameter while colliding, the collision can be different. When impact parameter (b) = 0; we would expect head-on or most central collision. In a collision, when the two nuclei touch each other slightly, that is a peripheral collision. This variation of collision depending on the impact parameter is called centrality. Centrality can be defined by the number of participating nuclei (N_{part}) or the binary nucleon collision number. The Glauber model can calculate the classes of centrality. In this chapter we learn about the basic constituents of matter in Standard Model, QCD

theory and its properties, concepts of QGP, High Energy Heavy-ion collisions, its evolution and its observables. In the next chapter we will discuss about how we can use Hydrodynamics as a model to process QGP properties.

Chapter 2

Hydrodynamics

QGP behaves like a superfluid, and we are supposed to get some fluid-like properties like pressure, temperature, specific heat, thermal conductivity, transport co-efficient etc. of it, but unfortunately, we do not have complete access to its properties; rather, we are only provided with the information about the spectra of final state particles. So, to estimate QGP properties, we need a theoretical model. Hydrodynamics describes continuous media, which shows collective behaviour and works in local thermal equilibrium region. For QGP, only the collective flow of the system as fluid is tractable, and its properties can also be measured at local equilibrium. To predict its behaviour, we can use hydrodynamics (in the relativistic region) as a suitable model.

2.1 Formulation of Relativistic Hydrodynamics

2.1.1 Prequisites

When two nuclei-nuclei collision happens it goes into three stages:

1. Initial state: While after colliding the excited hadrons or partons form fireball and try to reach a local equilibrium state (Thermalization state).
2. Expansion state: While fireball starts to expand and cools off due to pressure gradient, After reaching a certain critical temperature ($T_{cr} = 200$ MeV), the deconfinement-confinement phase transition happens until all partons turns into hadronic matter.
3. Freezeout state: In this stage hadronic interaction takes place, but after a while, the scattering tends to less as the distance between two partons for different hadrons

becomes greater than hadronic radius - thus kinetic freezeout happens and all the low mass particles come out (particle number now become fixed).

In heavy-ion collisions, a hydrodynamic approach can only be applicable during a finite interval between thermalization and freeze-out. It can never predict the early stages of collision. So, to obtain a phenomenologically suitable result we must include initial, final conditions and an equation of state in hydrodynamic model.

2.1.2 Relativistic Hydrodynamics from kinetic theory

Kinetic theory describes a medium microscopically, where the evolution of the phase-space distribution function follows $f(x, p, t)$, lorentz scalar that with four-momentum p^μ at space-time position x^μ . When collision comes into picture number of particles changes in ranges $\Delta^3 p$, $\Delta^4 x$ and it will be $\frac{\Delta^3 p}{p^0} \Delta^4 x C(x, p)$. Before solving $C(x, p)$ we assume that only 2 particles interact $(p_1^\mu, p_2^\mu) \rightarrow (p_1'^\mu, p_2'^\mu)$ and according to molecular chaos hypothesis, the average number of collisions in $\Delta^4 x$ is equal to $\frac{W(p_1^\mu p_2^\mu | p_1'^\mu p_2'^\mu)}{(p_1^0 p_2^0 p_1'^0 p_2'^0)} f(x, p_1) f(x, p_2) d^3 p_1 d^3 p_2$ (where assume $f(x, p)$ varies slowly in space and time). So after calculating total number of particle loss and gain we can get the transport equation as:

$$p^\mu \partial_\mu f(x, p) = \frac{1}{2} \iiint \frac{d^3 p_2}{p_2^0} \frac{d^3 p_1'}{p_1'^0} \frac{d^3 p_2'}{p_2'^0} [f_1' f_2' W(p_1' p_2' | p_1 p_2) - f_1 f_2 W(p_1 p_2 | p_1' p_2')] \quad (2.1)$$

$$= C[f]$$

here $C(x, p)$ is the collision term in which the strength of the interaction enters through their scattering cross sections. In Boltzmann equation, we can find an important property of this collision term [10]:

$$\int \frac{d^3 p}{p^0} \psi(x, p) C(x, p) = 0 \quad (2.2)$$

where $\psi(x, p) = a(x) + b_\mu(x) p^\mu$ is summational invariant. Now if $\psi(x, p) = a(x)$ in above equation :

$$\int \frac{d^3 p}{p^0} a(x) p^\mu \partial_\mu f(x, p) = 0 \implies \partial_\mu N^\mu = 0 \quad (2.3)$$

and if $\psi(x, p) = b_\mu(x) p^\mu$ it will give :

$$\int \frac{d^3 p}{p^0} b_\mu(x) p^\mu p^\nu \partial_\nu f(x, p) = 0 \implies \partial_\mu T^{\mu\nu} = 0 \quad (2.4)$$

Where equations 4.2 and 4.3 are the basic equations of hydrodynamics.

2.2 Relativistic Hydrodynamics Equation of Motion

In hydrodynamic we introduce flow velocity as $u^\mu = (\gamma, \gamma\vec{u})$ and its projector tensor $\Delta^{\mu\nu} = (g^{\mu\nu} - u^\mu u^\nu)$ and it holds the properties like $\Delta^{\mu\nu} u_\nu = 0$ and $u^\mu u_\mu = 1$. Hydrodynamic flow velocity can be calculated in two different way:

1. Eckart's flow: It is related to particle flow and defined by:

$$u^\mu = \frac{N^\mu}{\sqrt{N^\nu N_\nu}}; \text{ here } \Delta^{\mu\nu} N_\nu = 0$$

2. Landau and Lifshitz flow: It is related to the energy flow and can be defined by:

$$u^\mu = \frac{T^{\mu\nu} u_\nu}{u_\rho T^{\rho\sigma} u_\sigma}; \text{ here } \Delta^{\mu\nu} u_\nu = 0$$

At high energy level, Landau and Lifshitz definition of velocity is applied as mostly in RHIC, we have energy and momentum distributions as observables.

Hydrodynamics basic equation comes from energy-momentum conservation and current conservation equations [16], [8]:

$$\partial_\mu T^{\mu\nu}(x) = 0 \quad (2.5)$$

$$\partial_\mu N_i^\mu(x) = 0; i = 1, 2, 3..M \quad (2.6)$$

Along with second thermodynamic law:

$$\partial_\mu S^\mu(x) \geq 0 \quad (2.7)$$

Energy-momentum tensor $T^{\mu\nu} = eu^\mu u^\nu - p\Delta^{\mu\nu} + [(q^\mu + h\Delta^{\mu\tau} N_\tau)u^\nu + (q^\nu + h\Delta^{\nu\tau} N_\tau)u^\mu] + \Pi^{\mu\nu}$, charge current $N_i^\mu = n_i u^\mu + \Delta^{\mu\nu} N_{\nu,i} = n_i u^\mu + V_i^\mu$ and entropy of the system $S^\mu = su^\mu$; where e = energy density, p = hydrostatic pressure, q^μ = heat flow, h = enthalpy, $\Pi^{\mu\nu}$ = viscous pressure tensor, s = entropy density, $g^{\mu\nu} = (1, -\vec{1})$.

However for ideal case, dissipative terms like q^μ , $\Pi^{\mu\nu}$ and V^μ term goes to zero and in local rest frame ($u^\mu = \gamma(1, \vec{0})$):

$$T^{\mu\nu}(x) = (e(x) + p(x))u^\mu(x)u^\nu(x) - p(x)g^{\mu\nu} \text{ and } N^\mu(x) = n(x)u^\mu(x)$$

It has 7 variables (i.e; e, p, n, u^μ) and along with $u^\mu u_\mu = 1$ and EOS ($p = p(e, n)$), equations 2.5 and 2.6 gives rise to 7 equations which is solvable. If local relaxation rates are not fast enough to state it as a local thermalization, the dissipative terms includes in energy-momentum tensor ($T^{\mu\nu}$) and charge current (N^μ). Furthermore these terms are proportional to transport coefficient for diffusion, heat conductance, bulk and shear viscosity - solving these kind of equations are quite complicated. We need to introduce relaxation time and viscous correction term to solve it analytically [11], [31], [24], [9].

2.3 Applicability and length scale of Hydrodynamics

In equation 2.1, we have describe Boltzmann transport function with $C(x, p)$ and it can be further simplified in classical kinetic theory as:

$$C(x, p) = \frac{p^\mu u_\mu(x)}{\tau_{rel}(x, p)} [f_{eq}(x, p) - f(x, p)] \quad (2.8)$$

where the relaxation time $= \tau_{rel}$ and it generally depends on position through the local density and p^μ through the local rest frame energy of the particles.

- Classical kinetic theory is valid in the region where mean free path ($\lambda_{mfp} = < (p/E)\tau_{rel} >$) is large so, the particle interaction must not weak.
- Hydrodynamics is valid if the system is close enough to thermal equilibrium that its local momentum distribution (particle and energy density, pressure, which can all be expressed as moments of the local momentum distribution) can be characterized by a small number of thermodynamic and transport parameters. To treat the ensemble of particles as a single fluid, the mean free path of the particles must be significantly less than any other length scales of interest to us. So, it is applicable for strongly interacting constituents.

Based on ratio of the two microscopic length scales ($\frac{\lambda_{mfp}}{\lambda_{th}}$ (where λ_{th} = thermal wavelength) $\sim 1/T$ or η/s) we can define three regimes of microscopic dynamics:

(here η = shear viscosity, s = entropy density)[16]

1. **Dilute Gas regime:** Here $\frac{\lambda_{mfp}}{\lambda_{th}} \sim \frac{\eta}{s} \gg 1$;

This is weakly interacted regime and its motion is described by Boltzmann equation.

2. **Densed Gas regime:** $\frac{\lambda_{mfp}}{\lambda_{th}} \sim \frac{\eta}{s} \sim 1$;

The interaction can occur in λ_{th} scale. Here quantum kinetic approach based on Wigner distribution is taken.

3. **Liquid regime:** $\frac{\lambda_{mfp}}{\lambda_{th}} \sim \frac{\eta}{s} \ll 1$;

It is strongly interacted regime, hydrodynamics equation is applicable here.

But rather than simply saying hydrodynamics is only applicable for $\frac{\eta}{s} \ll 1$, it is more appropriate to say that it truly depends on Knudsen number ($K_n = \frac{\eta}{s} \cdot \frac{\theta}{T}$; $\theta = \partial_\mu u^\mu =$ inverse of the scalar expansion rate) and that is approximately 0 (ideal fluid) or less than equal to 1 (viscous fluid). For $K_n \gg 1$, hydrodynamic regime breaks.

Chapter 3

Various modes for calculating shear viscosity over entropy density ratio

Viscosity plays an important role in many regimes of physics like- atomic systems, nuclear matter, neutron star physics, low energy to relativistic energy heavy-ion collisions and at the extreme end string theory, so understanding it has become an interest of many domains. In RHIC, viscosity comes into the picture in QGP like phenomena (collective flow phenomena). According to microscopic kinetic theory, shear viscosity (η) describes the momentum transfer due to the particle thermal motion. It depends on the particle elastic scattering or interactions through the mean free path. It also gives a better estimate of the strength of interaction between molecules if their inter-spacing is the same. If the interaction is strong and the scattering cross-section is big, shear viscosity becomes small like in QGP; due to strong interaction between quarks and gluons, we expect small shear viscosity. We can call low viscous fluids, which interact strongly as nearly perfect fluids. If we can verify low viscosity or shear viscosity over entropy density ratio (η/s) in QGP, we can conclude that QGP is also a nearly perfect fluid. Although through AdS/CFT string theory η/s can have a lower limit up to $\hbar/(4\pi k_B)$ [18], [21] where k_B = Boltzmann constant, $\hbar = h/(2\pi)$ = Planck's constant we need to estimate the value or range of η/s in QGP state experimentally (This ratio in natural units is dimensionless).

3.1 UrQMD Box Calculation

Here we can use the UrQMD model to simulate η for infinite equilibrated hadronic particles. We confined the particles in a box with a periodic condition where they achieve equilibrium through only elastic collisions. Here we assume hadronic particles as hard sphere. We can find shear viscosity coefficient (η) as a function of temperature and baryo-chemical potential through Green-Kubo formalism [12].

$$\eta = \frac{V}{T} \int_0^\infty dt \langle \pi^{xy}(\vec{r}, t) \pi^{xy}(\vec{0}, 0) \rangle_{equilibrium} \quad (3.1)$$

where T = temperature of the system, t = post-equilibrium time (here $t = 0$ as the time the system equilibrates), π^{xy} = shear component of the energy-momentum tensor ($T^{\mu\nu}$). Here energy-momentum tensor ($T^{\mu\nu}$) defined as:

$$T^{\mu\nu} = \int d^3p \frac{p^\mu p^\nu}{p^0} f(x, p) \quad (3.2)$$

here p^μ = energy-momentum four vector, $\mu = 0, 1, 2, 3$, $f(x, p)$ = phase space density of the particles in the system.

In this case hadrons are treated as point particles uniformly distributed in coordinate space and thus we can write π^{xy} as [25]:

$$\pi^{xy} = \frac{1}{V} \sum_{i=1}^{N_{part}} \frac{p^x(i) p^y(i)}{p^0(i)} \quad (3.3)$$

where V = volume of the system. $\langle \pi^{xy}(\vec{r}, t) \pi^{xy}(\vec{0}, 0) \rangle$ = the correlations of the shear component of the energy momentum tensor and it is empirically found to be fitted with decay function with time [22].

3.2 Viscosity of Gas in Classical Approach

The viscosity for ordinary gases is assumed to depend on number density, mean free path and average momentum of the distribution [26].

$$\eta \approx n m v_{th} \lambda \approx n \langle |p| \rangle \lambda \quad (3.4)$$

Here n = number density, m = mass of the particle, λ = mean free path, v_{th} = thermal velocity, $\langle |p| \rangle$ = average momentum of the system.

3.3 Formulation of Viscosity of Hadron Gas

The viscosity a system of hadrons can be determined in a manner similar to the one carried out for ordinary gasses and it also depends on similar parameters that are mentioned above for classical gasses; here the only difference is that it is calculated in the relativistic domain and the hadron gasses are either fermions or bosons. So, for relativistic hadrons average momentum of the system (we consider Maxwell-Boltzmann Distribution):

$$\langle |p| \rangle = \frac{\int_0^\infty dp p^3 e^{-\frac{\sqrt{m^2+p^2}}{T}}}{\int_0^\infty dp p^2 e^{-\frac{\sqrt{m^2+p^2}}{T}}} \quad (3.5)$$

We can also rewrite denominator of the above equation i.e; total number of particles as a form of modified Bessel function of 2nd kind [27]:

$$\begin{aligned} \int_0^\infty dp p^2 e^{-\frac{\sqrt{m^2+p^2}}{T}} &= m^3 \int_0^\infty dx \sinh^2 x \cosh x e^{-\frac{m}{T} \cosh x} \\ &= m^2 T K_2\left(\frac{m}{T}\right) \end{aligned} \quad (3.6)$$

Now we can also rewrite the numerator of the equation 3.5 as a form of modified Bessel function of 2nd kind:

$$\begin{aligned} \int_0^\infty dp p^3 e^{-\frac{\sqrt{m^2+p^2}}{T}} &= m^4 \int_0^\infty dx \sinh^3 x \cosh x e^{-\frac{m}{T} \cosh x} \\ &= T^4 \frac{2^3/2m^5/2}{\sqrt{\pi}T} \left(\frac{3T}{2m} K_{3/2}\left(\frac{m}{T}\right) - K'_{3/2}\left(\frac{m}{T}\right) \right) \\ &= T^4 \frac{2^3/2}{\sqrt{\pi}} \left(\frac{m}{T}\right)^{5/2} K_{5/2}\left(\frac{m}{T}\right) \end{aligned} \quad (3.7)$$

So the equation 3.5 as a form of modified Bessel function of 2nd kind:

$$\langle |p| \rangle = \sqrt{\frac{8mT}{\pi}} \frac{K_{5/2}\left(\frac{m}{T}\right)}{K_2\left(\frac{m}{T}\right)} \quad (3.8)$$

The final expression for the viscosity of a relativistic gas of identical hadrons (as in the form of equation 3.4 and assuming $\lambda \propto \frac{1}{r^2}$) is [26]:

$$\eta \approx \frac{5\sqrt{mT} K_{5/2}\left(\frac{m}{T}\right)}{64\sqrt{\pi} r^2 K_2\left(\frac{m}{T}\right)} \quad (3.9)$$

where r = radius of a hadron.

For doing more generalization, we can use any distribution function (f_i) to equation 3.5

$$\langle |p| \rangle = \frac{\int_0^\infty dp p^3 f_i}{\int_0^\infty dp p^2 f_i} \quad (3.10)$$

and without getting into second order modified bessel function we can write the equation 3.9 as:

$$\eta \approx \frac{5}{64\sqrt{8}r^2} \frac{\int_0^\infty dp p^3 f_i}{\int_0^\infty dp p^2 f_i} \quad (3.11)$$

3.4 Formulation of Viscosity from Hydrodynamical Approach

As we have discussed in the previous section, we can only get transverse momentum spectra by the experiments at RHIC, and we can also observe its finite change from its equilibrium. In addition, QGP produced in this experiments evolves non-homogeneously (as we can see elliptical flow as a signature of QGP). Therefore, in this system, spatial inhomogeneity persists, and global equilibrium can never be achieved. Due to these reasons, some thermodynamic observables can become non-extensive. So, we can incorporate non-extensivity in the relativistic Boltzmann transport equation (BTE) and use it to calculate transport coefficients such as shear viscosity. Here we assume that the system is in a non-equilibrium state, which loses its energy and simultaneously produces entropy and goes to a local q-equilibrium after a certain relaxation time (τ). Here we are also considering thermodynamically consistent Tsallis distribution. The BTE is given by [30], [17], [36], [37]:

$$\frac{\partial f_p}{\partial t} + v_p^i \frac{\partial f_p}{\partial x^i} + F_p^i \frac{\partial f_p}{\partial p^i} = I(f_p) \quad (3.12)$$

Besides relaxation time approximation (RTA), with the assumption of no external force, the collision integral ($I(f_p)$) can be written as:

$$I(f_p) \approx -\frac{(f_p - f_p^0)}{\tau(E_p)} \quad (3.13)$$

where v_p^i = velocity of the i^{th} particle, F_p^i = external force acting on that particle, $\tau(E_p)$ = relaxation time that can be treated as mean time between two successive collisions. f_p^0 = Tsallis distribution function near local rest frame which is given as:

$$f_p^0 = \left[1 + (q - 1) \left(\frac{E_p - \vec{p} \cdot \vec{u} - \mu}{T} \right) \right]^{\frac{-q}{q-1}} \quad (3.14)$$

where \vec{u} = fluid velocity, T = temperature, μ = chemical potential, q = extensive parameter. The stress-energy tensor can further divided into ideal ($T_0^{\mu\nu}$) and dissipative term ($T_{dis}^{\mu\nu}$). When we introduce hydrodynamical description to it, we can see both transport coefficients shear viscosity (η) and bulk viscosity (ζ) already exists in $T_{dis}^{\mu\nu}$ term which can expressed in local lorentz frame as:

$$T^{ij} = -\eta \left(\frac{\partial u^i}{\partial x^j} + \frac{\partial u^j}{\partial x^i} \right) - \left(\zeta - \frac{2}{3}\eta \right) \frac{\partial u^i}{\partial x^j} \delta^{ij} \quad (3.15)$$

In terms of distribution function we can write equation 3.15 as:

$$T^{ij} = \int \frac{d^3p}{(2\pi)^3} \frac{p^i p^j}{E^p} \delta f_p \quad (3.16)$$

where δf_p denotes deviation from q-equilibrium and can expressed in given way with the help of equations 3.12 and 3.13:

$$\delta f_p = -\tau(E_p) \left(\frac{\partial f_p}{\partial t} + v_p^i \frac{\partial f_p}{\partial x^i} \right) \quad (3.17)$$

Under the approximation of a steady flow such as $u^i = (u_x(y), 0, 0)$ and having temperature to be space-time independent we can write equation 3.15 as $T^{xy} = -\eta \partial u_x / \partial y$. So, putting $\mu = 0$ from equations 3.16 and 3.17 we can further simplify T^{xy} as:

$$T^{xy} = \left(-\frac{1}{T} \int \frac{d^3p}{(2\pi)^3} \tau(E^p) \left(\frac{p_x p_y}{E_p} \right)^2 q(f_p^0)^{\frac{2q-1}{q}} \right) \frac{\partial u_x}{\partial y} \quad (3.18)$$

Thus coefficient of shear viscosity (η) for a single component of hadronic matter can be expressed as:

$$\eta = \frac{1}{15T} \frac{d^3p}{(2\pi)^3} \tau(E^p) \frac{p^4 q}{E_p^2} q(f_p^0)^{\frac{2q-1}{q}} \quad (3.19)$$

Here relaxation time is expressed by:

$$\tau^{-1}(E_a) = \sum_{bcd} \int \frac{d^3p_b d^3p_c d^3p_d}{(2\pi)^3 (2\pi)^3 (2\pi)^3} W(a, b \rightarrow c, d) f_b^0 \quad (3.20)$$

Where E_a = energy of the a_{th} particle, f_b^0 = Tsallis distribution of b_{th} particle and transition rate from a,b to c,d; $W(a, b \rightarrow c, d)$ is given by:

$$W(a, b \rightarrow c, d) = \frac{2\pi^4 \delta(p_a + p_b - p_c - p_d)}{2E_a 2E_b 2E_c 2E_d} |M|^2 \quad (3.21)$$

where $|M|$ is transition amplitude and now if we take centre-of-mass frame then the equation 3.20 becomes:

$$\begin{aligned} \tau^{-1}(E_a) &= \sum_{bcd} \int \frac{d^3p_b}{(2\pi)^3} \sigma_{ab} \frac{\sqrt{s - 4m^2}}{2E_a 2E_b} f_b^0 \\ &\equiv \sum_b \int \frac{d^3p_b}{(2\pi)^3} \sigma_{ab} v_{ab} f_b^0 \end{aligned} \quad (3.22)$$

where v_{ab} = relative velocity, σ_{ab} = scattering cross section, \sqrt{s} = energy of centre-of-mass frame. If we take the averages relaxation time ($\tilde{\tau}$, averaging over f_a^0) then equation 3.22

can be further written as :

$$\begin{aligned}
\tilde{\tau}_a^{-1} &= \frac{\int d^3p_a (2\pi)^3 \tau^{-1}(E_a) f_a^0}{\int d^3p_a (2\pi)^3 f_a^0} \\
&= \sum_b \frac{\int \frac{d^3p_a d^3p_b}{(2\pi)^3 (2\pi)^3} \sigma_{ab} v_{ab} f_a^0 f_b^0}{\int d^3p_a (2\pi)^3 f_a^0} \\
&= \sum_b b n_b \langle \sigma_{ab} v_{ab} \rangle
\end{aligned} \tag{3.23}$$

where n_b = number density of the b_{th} particle. In all above equations have been estimated using a single hadron. Now if we do a thermal averaging over the scattering of all particles of same hadron species ($\langle \sigma_{ab} v_{ab} \rangle$) with a constant hadron collision cross-section (σ) and taking $\mu = 0$, we can write it as:

$$\langle \sigma_{ab} v_{ab} \rangle = \frac{\sigma \int d^3p_a d^3p_b v_{ab} e_q^{\frac{-E_a}{T}} e_q^{\frac{-E_b}{T}}}{\int d^3p_a d^3p_b e_q^{\frac{-E_a}{T}} e_q^{\frac{-E_b}{T}}} \tag{3.24}$$

We can further simplify the momentum space volume elements as :

$$d^3p_a d^3p_b = 8\pi^2 p_a p_b dE_a dE_b d(\cos \theta) \tag{3.25}$$

Now with the help of equation 3.25, equation 3.24 can be expressed as:

$$\langle \sigma_{ab} v_{ab} \rangle = \frac{\sigma \int 8\pi^2 p_a p_b dE_a dE_b e_q^{\frac{-E_a}{T}} e_q^{\frac{-E_b}{T}} \frac{\sqrt{(E_a E_b - p_a p_b \cos \theta)^2 - (m_a m_b)^2}}{E_a E_b - p_a p_b \cos \theta}}{\int 8\pi^2 p_a p_b dE_a dE_b e_q^{\frac{-E_a}{T}} e_q^{\frac{-E_b}{T}}} \tag{3.26}$$

Therefore equation 3.19 along with equations 3.20 to 3.26 is needed to calculate shear viscosity of a particular hadron species.

3.5 Entropy Density

According to Boltzmann, entropy can be defined as a measure of the number of possible microstates of a system in thermodynamic equilibrium. In general we treated entropy as a measure of randomness in a system and entropy density is an important physical quantity (intensive quantity) that measures entropy per unit volume of a system. From statistical thermodynamics (Gibbs formula) we can deduce entropy density (s) as:

$$s = \frac{\epsilon + P - \mu_B \rho_B}{T} \tag{3.27}$$

where ϵ = energy density, P = pressure, T = temperature, V = volume, μ_B = baryo-chemical potential, and ρ_B = number densities of the relevant chemical species at equilibrium system.

For most of the calculation we take μ_B as 0 so we can rewrite equation 3.27 as:

$$s = \frac{\epsilon + P}{T} \quad (3.28)$$

equation 3.27 can be written as differential form as [33]:

$$s = \left(\frac{\partial P}{\partial T} \right)_V \quad (3.29)$$

Here number density (n), pressure (P), energy density (ϵ) can be computed in integral form:

$$n = \frac{g}{(2\pi)^3} \int d^3p f_i \quad (3.30)$$

$$P = \frac{g}{(2\pi)^3} \int \frac{d^3p |\vec{p}|^2}{p^0} f_i \quad (3.31)$$

$$\epsilon = \frac{g}{(2\pi)^3} \int d^3p p^0 f_i \quad (3.32)$$

g = degeneracy factor

So equation 3.28 can be again rewritten with the help of equation 3.31 and equation 3.32 in an integral form. Here I have used Tsallis distribution where all f_i is practically f_i^q (I have use it as I also fitted p_T distribution with Tsallis) and defined by :

$$f_i^q = \left[1 + (q - 1) \left(\frac{E - \mu}{T} \right) \right]^{\frac{-q}{q-1}} \quad (3.33)$$

and the average number of particles (N) will be $N = \sum_i f_i^q$. Using equations 3.11 and 3.28 we can get η/s value for any hadron gas. Equations 3.11, 3.28, 3.30, 3.31, 3.32 can be written as with Tsallis distribution function of the form equation 3.33.

In this chapter we have discussed about the most possible way to calculate shear viscosity over entropy density ratio and for simplicity we have used classical formalism mentioned in equations 3.11 and 3.28. In this next chapters we will discuss about the the results that has been produced by using the UrQMD event generator [5], [7], [15].

Chapter 4

Result and Conclusion

Here I have worked with charged pion particles (π^\pm) and kaon particles (K^\pm).

4.1 Charged Pion Characteristics

Pid in UrQMD = 101 [3], [2]

mass = 139.57039 MeV

charge: +1 (π^+), -1 (π^-)

spin = 0

composition: $\pi^+(u\bar{d})$, $\pi^-(d\bar{u})$

charged radius: 0.3 fm [28]

4.2 Charged Kaon Characteristics

Pid in UrQMD = 106 (for K^+), -106 (for K^-)

mass= 493.677 MeV

charge: +1 (K^+), -1 (K^-)

spin = 0

composition: $K^+(u\bar{s})$, $K^-(s\bar{u})$

charged radius: 0.3 fm [28]

4.3 Computation

The expressions for calculating η/s value for any charged pion and kaon gas are equations 3.11 and 3.28. Here we are finding the η/s value in the regime between chemical and kinetic freeze-out where we are considering pions and kaons as hadron gas molecules which interact through elastic collision only. The dependency of η/s for various centrality would be also studied here. Here we are using the values of freeze-out temperature, volume, non-extensivity parameter (q) after fitting p_T distribution with Tsallis distribution. After getting the required parameters using C++ code and implicating equation 3.11 and 3.28, we have achieved shear viscosity and entropy density for charged pions and kaons for each centrality respectively. The results are tabulated in natural units.

Here the taken centralities of UrQMD data [4]:

| | | | | | | | |
|----------------------------|-------|-------|-------|-------|-------|-------|-------|
| Centality (%) | 0-5 | 5-10 | 10-15 | 15-20 | 20-25 | 25-30 | 30-35 |
| $\langle N_{part} \rangle$ | 383.4 | 331.2 | 281.2 | 239.0 | 202.1 | 169.5 | 141.0 |
| Centality (%) | 35-40 | 40-45 | 45-50 | 50-55 | 55-60 | 60-65 | 65-70 |
| $\langle N_{part} \rangle$ | 116.0 | 94.11 | 75.3 | 59.24 | 45.58 | 34.33 | 25.21 |

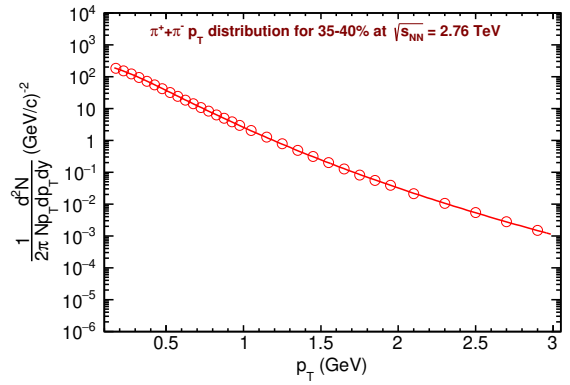
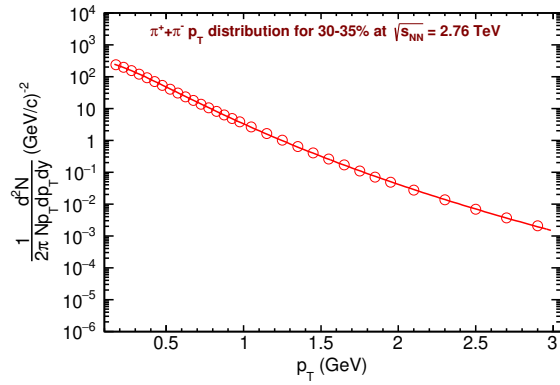
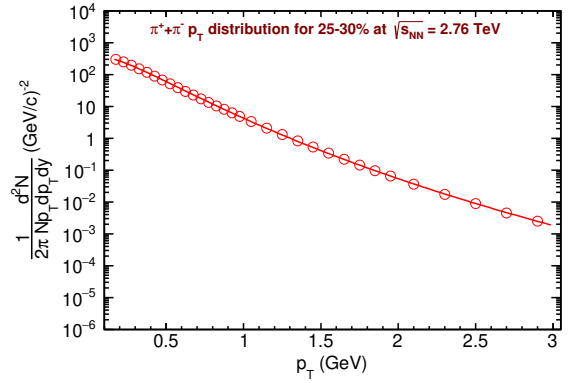
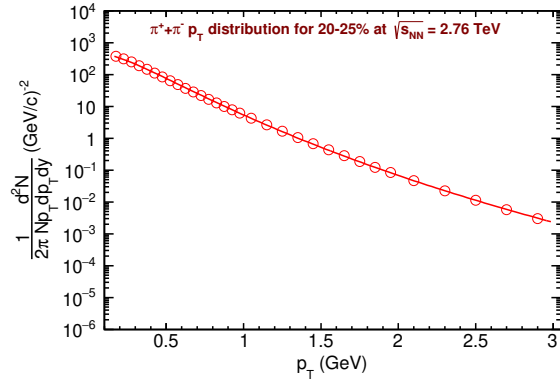
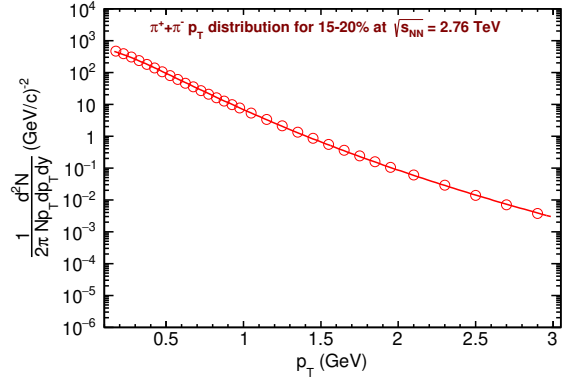
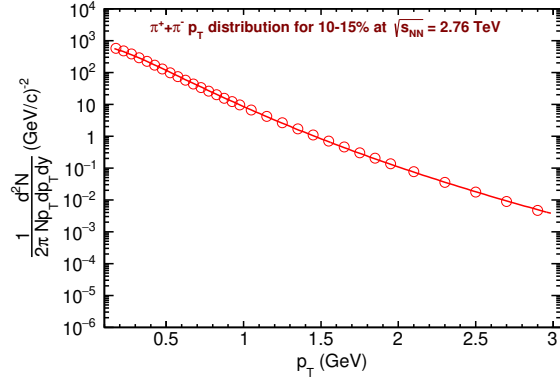
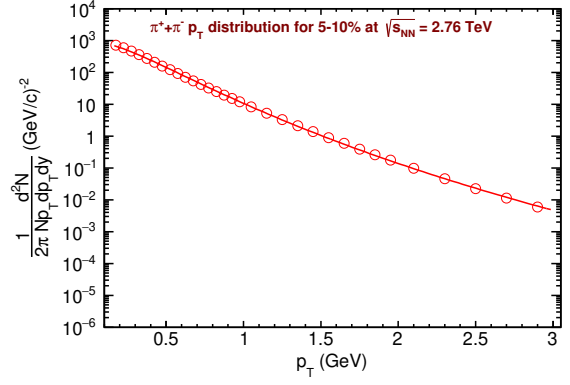
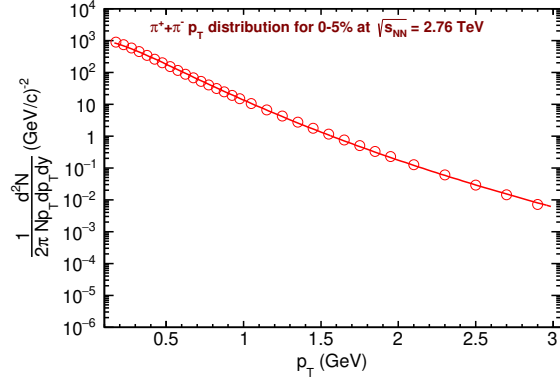
Table 4.1: $\langle N_{part} \rangle$ for each centrality class

| Centrality (%) | Temperature (T) (MeV) | q | Volume (V) ($X10^5 GeV^{-3}$) |
|-------------------|------------------------------|------------------------|------------------------------------|
| 0-5 | 108.849 ± 2.229 | 1.06944 ± 0.00216 | 70.1070 ± 5.5020 |
| 5-10 | 107.728 ± 2.210 | 1.07022 ± 0.00217 | 58.0405 ± 4.5537 |
| 10-15 | 107.171 ± 2.183 | 1.07011 ± 0.002169 | 47.8578 ± 3.7337 |
| 15-20 | 106.709 ± 2.164 | 1.07009 ± 0.002142 | 39.4185 ± 3.0634 |
| 20-25 | 105.520 ± 2.135 | 1.07102 ± 0.00214 | 32.9415 ± 2.5526 |
| 25-30 | 104.620 ± 2.119 | 1.07168 ± 0.00215 | 27.0833 ± 2.09400 |
| 30-35 | 102.894 ± 2.099 | 1.07317 ± 0.00217 | 22.5762 ± 1.7485 |
| 35-40 | 103.184 ± 2.075 | 1.07248 ± 0.00214 | 17.4662 ± 1.3383 |
| 40-45 | 103.183 ± 2.055 | 1.07193 ± 0.00212 | 13.3617 ± 1.0156 |
| 45-50 | 101.900 ± 2.070 | 1.07341 ± 0.00216 | 10.4394 ± 0.8038 |
| 50-55 | 98.794 ± 2.057 | 1.07749 ± 0.00225 | 7.2039 ± 0.5599 |
| 55-60 | 98.016 ± 2.052 | 1.07876 ± 0.00228 | 4.3300 ± 0.3363 |
| 60-65 | 96.192 ± 2.057 | 1.08166 ± 0.00234 | 3.1128 ± 0.2451 |

Table 4.2: Centrality wise Freeze-out parameters after fitting p_T spectra with Tsallis distribution for π^\pm for UrQMD data of Pb-Pb collision at $\sqrt{s_{NN}} = 2.76$ TeV

| centrality (%) | Temperature (T) (MeV) | q | Volume (V) ($\times 10^5 GeV^{-3}$) |
|-------------------|------------------------------|-----------------------|--|
| 0-5 | 163.157 ± 3.936 | 1.03325 ± 0.00294 | 3.9921 ± 0.3818 |
| 5-10 | 157.862 ± 3.906 | 1.03648 ± 0.00296 | 3.5537 ± 0.35086 |
| 10-15 | 152.955 ± 3.868 | 1.03923 ± 0.00295 | 3.1979 ± 0.3251 |
| 15-20 | 147.318 ± 3.852 | 1.04313 ± 0.00299 | 29.439 ± 0.3112 |
| 20-25 | 142.102 ± 3.825 | 1.04658 ± 0.00300 | 2.6887 ± 0.2947 |
| 25-30 | 136.621 ± 3.823 | 1.05064 ± 0.00301 | 2.46593 ± 0.2826 |
| 30-35 | 132.010 ± 3.774 | 1.05387 ± 0.00302 | 2.2022 ± 0.2603 |
| 35-40 | 126.432 ± 3.801 | 1.0822 ± 0.00310 | 2.0062 ± 0.2502 |
| 40-45 | 121.59 ± 3.788 | 1.06172 ± 0.00313 | 1.7795 ± 0.2318 |
| 45-50 | 115.352 ± 3.855 | 1.06732 ± 0.00325 | 1.6236 ± 0.2273 |
| 50-55 | 110.987 ± 3.859 | 1.07094 ± 0.00328 | 1.3702 ± 0.2010 |
| 55-60 | 109.549 ± 3.861 | 1.07211 ± 0.00329 | 1.0371 ± 0.1547 |
| 60-65 | 107.645 ± 3.819 | 1.07385 ± 0.00325 | 0.77416 ± 0.1170 |
| 65-70 | 102.391 ± 3.975 | 1.07964 ± 0.00347 | 0.6392 ± 0.1055 |

Table 4.3: Centrality wise Freeze-out parameters after fitting p_T spectra with Tsallis distribution for K^\pm for UrQMD data of Pb-Pb collision at $\sqrt{s_{NN}} = 2.76$ TeV



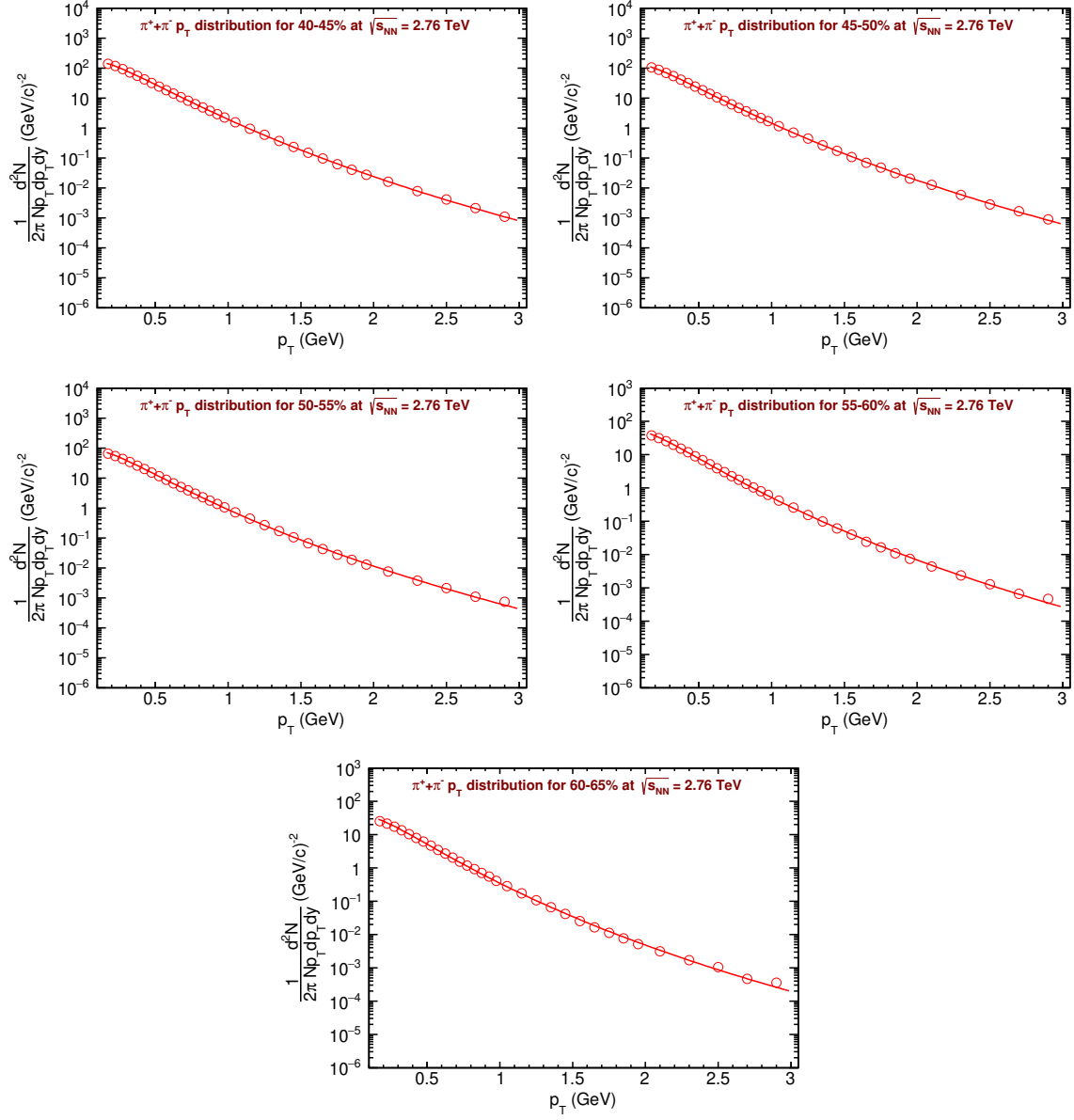
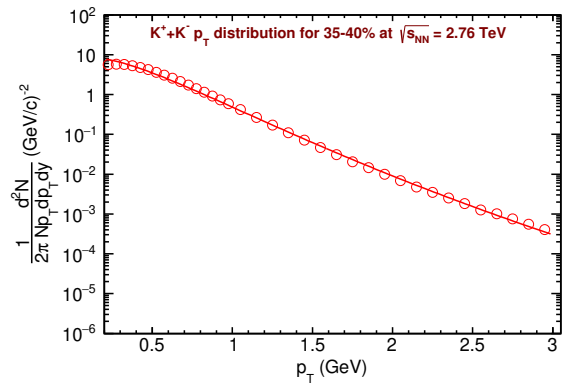
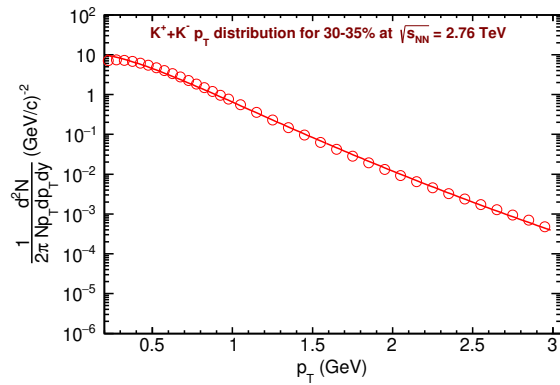
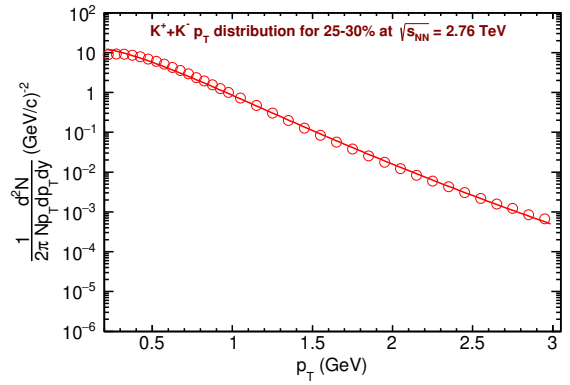
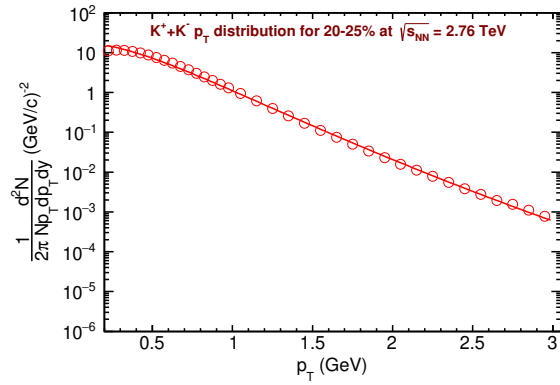
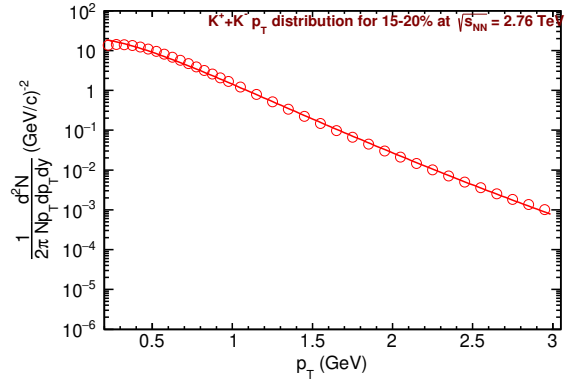
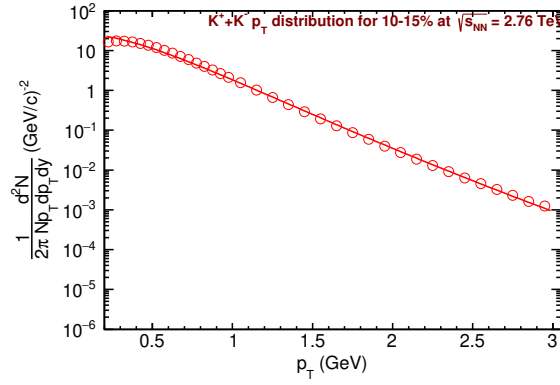
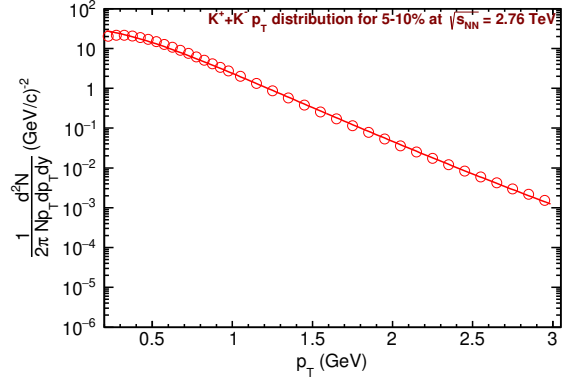
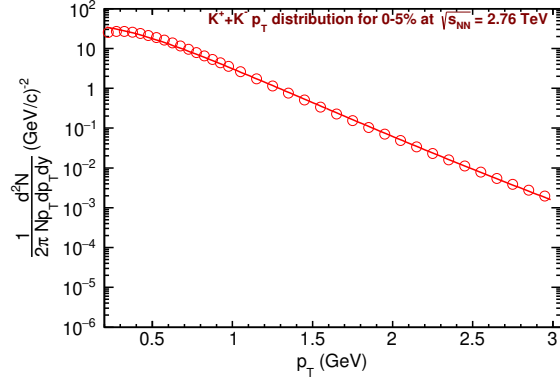


Figure 4.1: $\pi^+ + \pi^-$ (total) p_T distribution fitted with Tsallis for Pb-Pb collision energy at $\sqrt{s_{NN}} = 2.76$ TeV with $|\eta| \leq 0.5$ for different centrality (for UrQMD data)



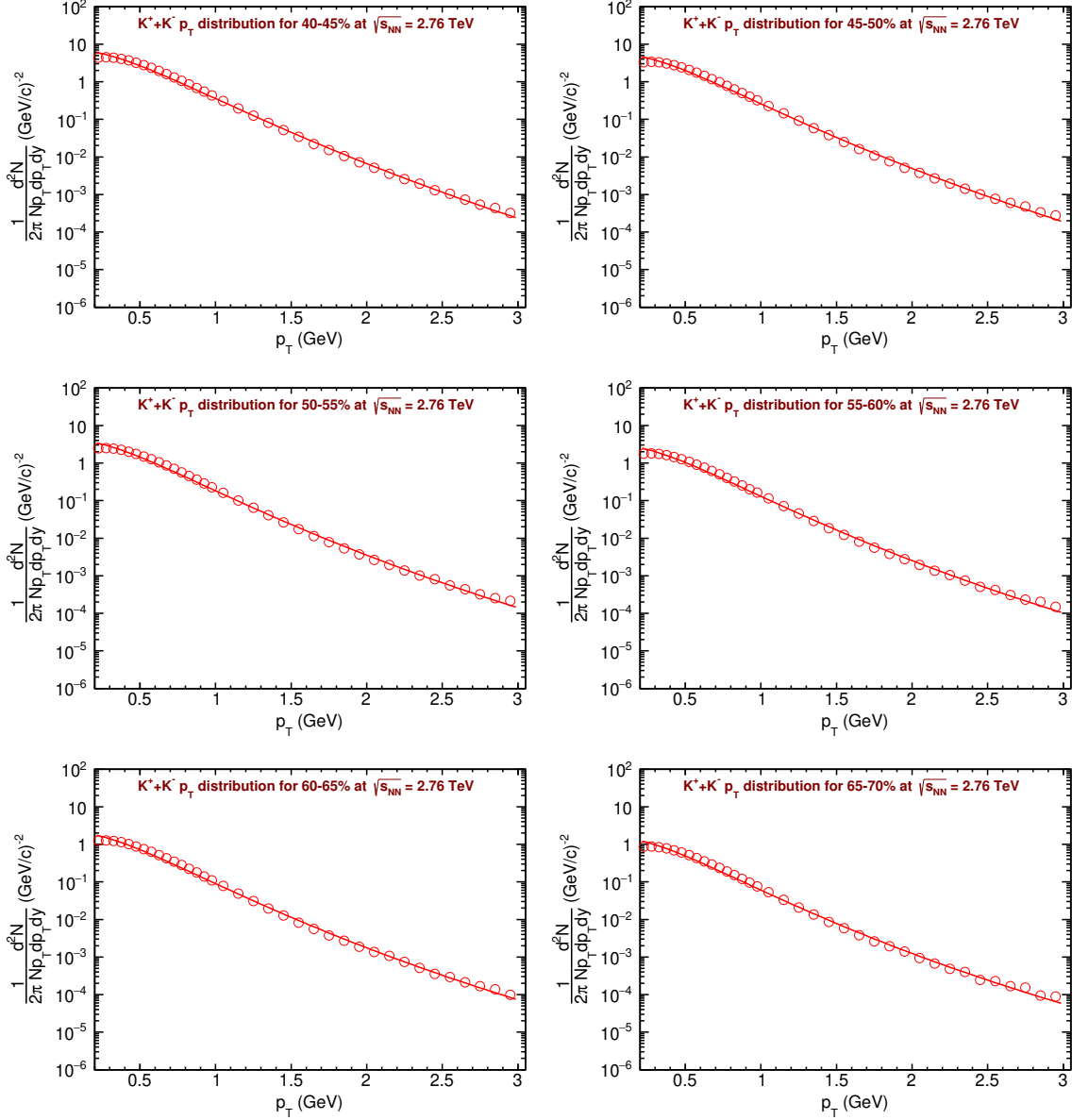


Figure 4.2: $K^+ + K^-$ (total) p_T distribution fitted with Tsallis for Pb-Pb collision energy at $\sqrt{s_{NN}} = 2.76$ TeV with $|\eta| \leq 0.5$ for different centrality (for UrQMD data)

We have used the centrality data of table 4.1 in our calculation. After fitting the transverse momentum spectra (figures 4.1 and 4.2 for charged pions and kaons respectively using UrQMD data) to Tsallis-Boltzmann distribution, we tabulated the required parameters like - temperature (T), non-extensive parameter (q) and volume (V). We are dealing with relatively small number of particles (a few thousands) compare to the system with Avogadro's number of particle. Here usual Boltzmann statistics is not quite fruitful. So, to apply statistical model and get a good approximation of thermodynamical observables in RHIC experiments, instead of using Boltzmann statistics, Tsallis statistics is a good alter-

native as the q parameter also take care of the non-extensivity of the system. We can also observe in tables 4.2 and 4.3 that there is a notable trend in non-extensive parameter (q) and temperature. As we approach to most central collisions, q decreases to 1 (when $q \rightarrow 1$; Tsallis statics and Boltzmann statics become equivalent) and temperature increases for charged pions as well as kaons. It also seems that there is a mass dependency with how the temperature increases, as we observe it is steeper for kaons than pions (kaons are heavier than pions).

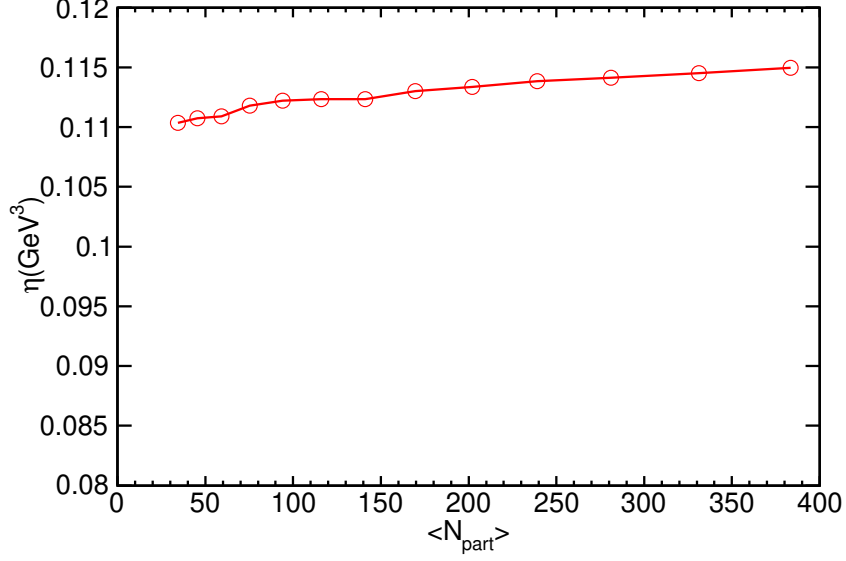


Figure 4.3: shear viscosity as varying $\langle N_{part} \rangle$ for $\pi^+ + \pi^-$ (total) p_T produced in Pb-Pb collision at $\sqrt{s_{NN}} = 2.76$ TeV with $|\eta| \leq 0.5$ for UrQMD data

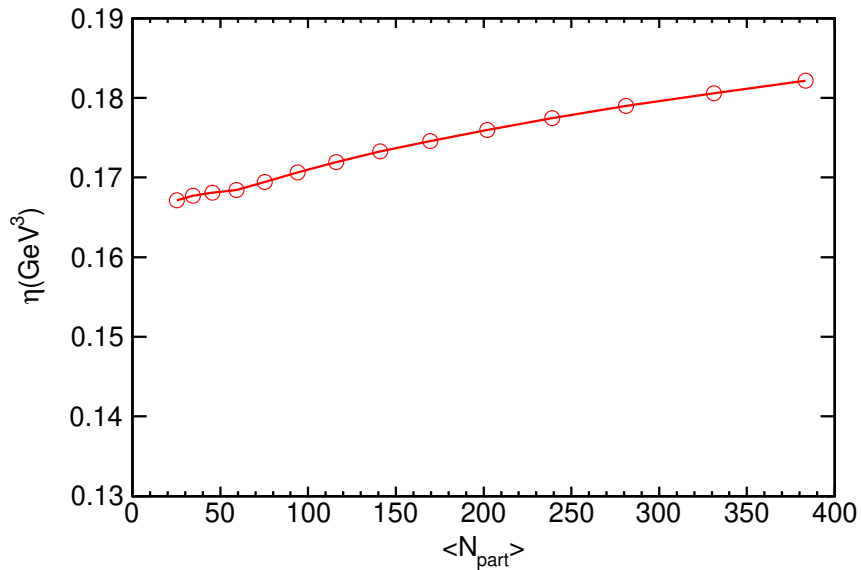


Figure 4.4: shear viscosity as varying $\langle N_{part} \rangle$ for $K^+ + K^-$ (total) p_T produced in Pb-Pb collision at $\sqrt{s_{NN}} = 2.76$ TeV with $|\eta| \leq 0.5$ for UrQMD data

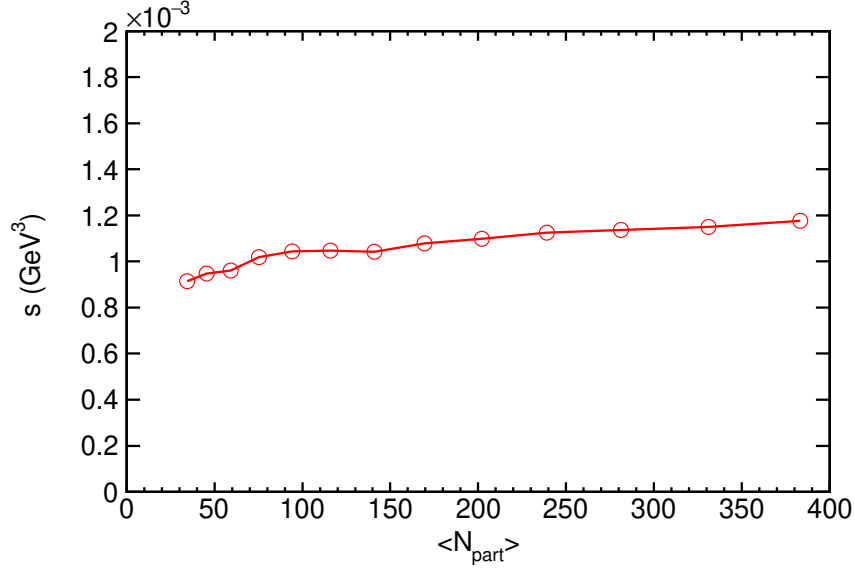


Figure 4.5: entropy density as varying $\langle N_{part} \rangle$ for $\pi^+ + \pi^-$ (total) p_T produced in Pb-Pb collision at $\sqrt{s_{NN}} = 2.76$ TeV with $|\eta| \leq 0.5$

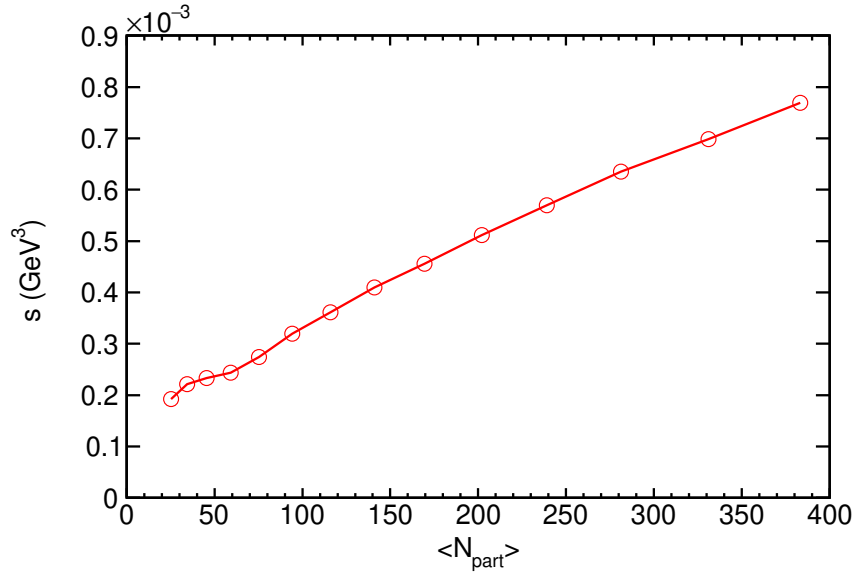


Figure 4.6: entropy density as varying $\langle N_{part} \rangle$ for $K^+ + K^-$ (total) p_T produced in Pb-Pb collision at $\sqrt{s_{NN}} = 2.76$ TeV with $|\eta| \leq 0.5$ for UrQMD data

We can see from figures 4.3, 4.4 and figures 4.5, 4.6 that for both pions and kaons shear viscosity and entropy density are subtly increasing for higher N_{part} i.e; near to most central values where the particle density is the most. From crude kinetic theory of gas (equation 3.4) we can conclude that if number density of a system increases, momentum transfer due

to the particle thermal motion increases and ultimately shear viscosity increases. Similar effect seen in entropy density as particle density increases.

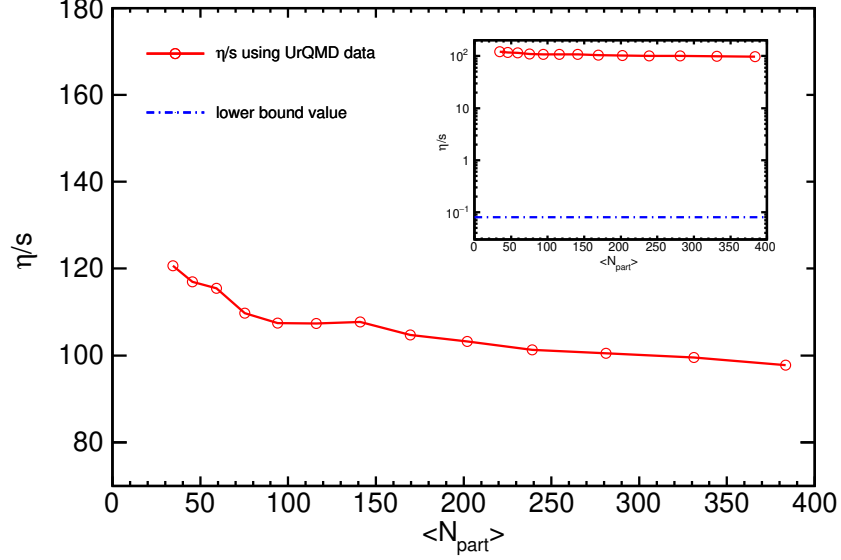


Figure 4.7: shear viscosity over entropy density ratio as varying $\langle N_{part} \rangle$ for $\pi^+ + \pi^-$ (total) p_T produced in Pb-Pb collision at $\sqrt{s_{NN}} = 2.76$ TeV with $|\eta| \leq 0.5$ for UrQMD data

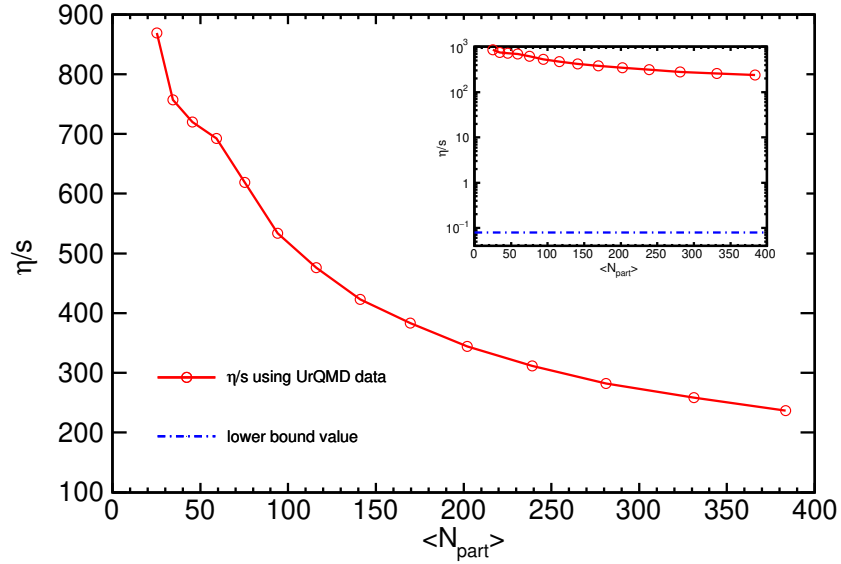


Figure 4.8: shear viscosity over entropy density ratio as varying $\langle N_{part} \rangle$ for $K^+ + K^-$ (total) p_T produced in Pb-Pb collision at $\sqrt{s_{NN}} = 2.76$ TeV with $|\eta| \leq 0.5$ for UrQMD data

From figures 4.7 and 4.8 we can deduct that shear viscosity over entropy density ratio for both charged pions and kaons are decreasing towards KSS bound. Although in figures

4.3, 4.4 and figures 4.5, 4.6; both shear viscosity and entropy density increases in most central collision, but due to the rapid increase in entropy density, the whole ratio shows the opposite trend. It can be thought such that as the system comprising of only elastically interacted hard sphere hadron particles is produced by most central collisions, the particle density increases and the system behaves like more of a QGP like one. The values of η/s for these hadron gasses(charged pions and kaons), shown in inlay of figures 4.5 and 4.6 [the blue dashed line is KSS bound] are not in the range of 0.08 to 0.24 (predicted from AdS/CFT string theory) as we initially assumed only elastic collision where these hadrons are interacting elastically throughout chemical freeze-out to kinetic freeze-out. So, we would not expect to get shear viscosity over entropy density ratio to be of QGP's. But we can say that compare to kaons, the shear viscosity over entropy density ratio for pions are more close to the lower bound.

Chapter 5

Summary and Conclusion

From the beginning, our aim was to study one of the QGP properties like shear viscosity over entropy density ratio in a model-based system, as we cannot have direct access to these. So at first, we try to familiarize ourselves with the standard model, quarks, gluons. Then the concept of QGP comes into the picture. There we study the dynamics of QGP, i.e., QCD (Quantum Chromo Dynamics). Next, we focus on creating QGP like phenomena in a lab environment in Relativistic Heavy-ion collision (RHIC). Then we quickly go through the evolution of collision in RHIC and its observables. Later, we directly go to the models from which we can extract shear viscosity over entropy density ratio analytically. We have been introduced to three different methods- classical approach, UrQMD box model and hydrodynamical approach. Here I have used the most simplistic one-classical approach and studied in Pb-Pb collisions at $\sqrt{s_{NN}} = 2.76$ TeV using UrQMD event generator and obtained a trend in centrality fluctuations. With a significant assumption of only taking elastic collisions in hadronic particles, which are assumed as hard sphere, we have studied η/s for charged pions and kaons as they are the most produced final state particles ($> 70 - 80\%$). We have fitted charged pion and kaon spectra at different centrality with Tsallis-Boltzmann distribution to extract temperature, non-extensive parameter (q) and volume for our calculation purpose. Generally, we use Boltzmann statistics to those systems, comprising of a large number of particles nearly of the order of Avogadro's number. But in this scenario (RHIC), we have a few numbers (around some thousands) of particles in the system. Hence, using Tsallis-Boltzmann distribution seems quite effective as its extensive parameter (q) takes care of this crisis. We have observed a notable variation in q over centrality as we go towards the most central collisions, q value decreases to 1 for both charged particles; as if

the system produced by most central collision (they have a significant number of particles in the system compare to other collisions and nearly close to Avogadro's number) tries to achieve thermodynamical equilibrium. For temperature, it exhibits the opposite trend for both charged particles but for charged kaons; it is slightly steeper than charged pions so, there might have some mass dependency to it. We have also seen that for both charged particles, shear viscosity and entropy density increases as we go towards most central collision whereas shear viscosity over entropy density ratio (η/s) shows the opposite trend. This is plausible as for most central collisions, hadron particle density increases, creating a more of a QGP (hot and dense partons) like situation. Although the values are not close to that of QGP, we can observe that the values for charged pions are closer than that of charged kaons. For further modification, we can use the relativistic Boltzmann transport equation to calculate shear viscosity as it includes the principle of relativistic hydrodynamics as well as dissipation terms.

Appendix A

Simulating the Events: Technical Part

We have written a set of codes using 'c++' programming language and which uses ROOT classes. Following are the main components of this monte carlo simulations.

- 1: The yields of individual particles are estimated from already published p_T spectra of each particle.
- 2: A monte-carlo event generator is written to generate both positive and negative particles.
- 3: Several parallel jobs are submitted to IISER Mohali HPC facility via a newly written qsub script
- 4: Further these outputs are collected and fed into a newly written parsing code to produce the plots.

Bibliography

- [1] *Evolution of collisions and qgp.*
- [2] *Urqmd manual.*
- [3] *Urqmd user guide.*
- [4] *Centrality determination in heavy ion collisions*, (2018).
- [5] S. A. BASS ET AL., *Microscopic models for ultrarelativistic heavy ion collisions*, Prog. Part. Nucl. Phys., 41 (1998), pp. 255–369.
- [6] A. BHATTACHARYYA, S. DAS, S. K. GHOSH, S. RAHA, R. RAY, K. SAHA, AND S. UPADHAYA, *Net Charge Fluctuations as a signal of QGP from Polyakov-Nambu-Jona-Lasinio model*, (2012).
- [7] M. BLEICHER ET AL., *Relativistic hadron hadron collisions in the ultrarelativistic quantum molecular dynamics model*, J. Phys. G, 25 (1999), pp. 1859–1896.
- [8] M. BORSHCH AND V. ZHDANOV, *Exact solutions of the equations of relativistic hydrodynamics representing potential flows*, Symmetry, Integrability and Geometry: Methods and Applications (SIGMA), 3 (2007).
- [9] M. S. BORSHCH AND V. I. ZHDANOV, *Exact solutions of the equations of relativistic hydrodynamics representing potential flows*, SIGMA, 3 (2007), p. 116.
- [10] A. CHAUDHURI, *A short course on relativistic heavy ion collisions*, (2012).
- [11] A. K. CHAUDHURI, *Viscous Hydrodynamic Model for Relativistic Heavy Ion Collisions*, Adv. High Energy Phys., 2013 (2013), p. 693180.
- [12] N. DEMIR AND S. BASS, *Shear-viscosity to entropy-density ratio of a relativistic hadron gas*, Physical review letters, 102 (2009), p. 172302.

- [13] S. HELMUT, *The Thermodynamics of Quarks and Gluons*, Lect. Notes Phys., 785 (2010), pp. 1–21.
- [14] W.-Y. P. HWANG AND S. P. KIM, *Phase transitions in the early universe*, 2017.
- [15] A. JAISWAL AND V. ROY, *Relativistic hydrodynamics in heavy-ion collisions: general aspects and recent developments*, Adv. High Energy Phys., 2016 (2016), p. 9623034.
- [16] S. JEON AND U. HEINZ, *Introduction to Hydrodynamics*, Int. J. Mod. Phys. E, 24 (2015), p. 1530010.
- [17] G. P. KADAM AND H. MISHRA, *Dissipative properties of hot and dense hadronic matter in an excluded-volume hadron resonance gas model*, Phys. Rev. C, 92 (2015), p. 035203.
- [18] P. K. KOVTUN, D. T. SON, AND A. O. STARINETS, *Viscosity in strongly interacting quantum field theories from black hole physics*, Physical Review Letters, 94 (2005).
- [19] R. LYDAHL, *Elliptic flow studies using event shape engineering in pb-pb collisions at alice*, 2017.
- [20] P. S. MAHALLE, *Equation of state for quark gluon plasma*.
- [21] A. MEKJIAN, *Viscosity of a nucleonic fluid*, (2012).
- [22] A. MOTORNENKO, L. BRAVINA, M. GORENSTEIN, A. MAGNER, AND E. ZABRODIN, *Nucleon matter equation of state, particle number fluctuations, and shear viscosity within UrQMD box calculations*, J. Phys. G, 45 (2018), p. 035101.
- [23] C. NATTRASS, *Measurements of jets in heavy ion collisions*, EPJ Web of Conferences, 172 (2018), p. 05010.
- [24] J.-Y. OLLITRAULT, *Relativistic hydrodynamics for heavy-ion collisions*, Eur. J. Phys., 29 (2008), pp. 275–302.
- [25] S. PAL, *Shear viscosity to entropy density ratio of a relativistic Hagedorn resonance gas*, Phys. Lett. B, 684 (2010), pp. 211–215.
- [26] M. S. PRADEEP, *Shear viscosity of a hadron gas*.

- [27] W. PUBLICATION, *Bessel functions of the first and second kind*.
- [28] RIAZUDDIN, *Charge radius of pion*, Phys. Rev., 114 (1959), pp. 1184–1186.
- [29] R. SAHOO, *Relativistic kinematics*, 2016.
- [30] D. SAHU, S. TRIPATHY, R. SAHOO, AND A. R. DASH, *Multiplicity dependence of shear viscosity, isothermal compressibility and speed of sound in pp collisions at $\sqrt{s} = 7 \text{ TeV}$* , European Physical Journal A, 56 (2020), p. 187.
- [31] S. SARKAR, H. SATZ, AND B. SINHA, eds., *The physics of the quark-gluon plasma*, vol. 785, 2010.
- [32] H. SATZ, *The thermodynamics of quarks and gluons*, Lecture Notes in Physics, (2009), p. 1–21.
- [33] J. SCHMALIAN, *Lecture notes, statistical mechanics*.
- [34] A. SIRUNYAN, A. TUMASYAN, W. ADAM, F. AMBROGI, T. BERGAUER, J. BRANDSTETTER, M. DRAGICEVIC, J. ERÖ, A. ESCALANTE DEL VALLE, M. FLECHL, AND ET AL., *Running of the top quark mass from proton-proton collisions at $s=13\text{TeV}$* , Physics Letters B, 803 (2020), p. 135263.
- [35] R. SNELLINGS, *Elliptic flow: a brief review*, New Journal of Physics, 13 (2011), p. 055008.
- [36] S. K. TIWARI, S. TRIPATHY, R. SAHOO, AND N. KAKATI, *Dissipative properties and isothermal compressibility of hot and dense hadron gas using non-extensive statistics*, European Physical Journal C, 78 (2018), p. 938.
- [37] G. D. YEN, M. I. GORENSTEIN, W. GREINER, AND S. N. YANG, *Excluded volume hadron gas model for particle number ratios in $A + A$ collisions*, Phys. Rev. C, 56 (1997), pp. 2210–2218.
- [38] A. R. ZHITNITSKY, *Confinement–deconfinement phase transition in hot and dense qcd at large n* , Nuclear Physics A, 813 (2008), p. 279–292.